The effects of the temperature in the testing system on the measurements of thermal rock strain with clip-on extensometers

L. Pei[a,b], G. Blöcher[b], Y. J. Wang[a,*], H. Milsch[b], G. Zimmermann[b], E. Huenges[b], W. Xiang[c]

[a] Wuhan Institute of Technology, School of Civil Engineering and Architecture, Optics Valley, 430205 Wuhan, China

[b] Helmholtz-Zentrum Potsdam-Deutsches GeoForschungsZentrum GFZ, Telegrafenberg, 14473 Potsdam, Germany

[c] China University of Geosciences (Wuhan), Three Gorges Research Center for Geohazards, Ministry of Education, Lumo Road, 430074 Wuhan, China

*Corresponding author: Y. J. Wang

E-mail address: witpcw@126.com

Highlights

- Heterogeneous temperature distributed in the testing system
- Plug-in temperature yielded the apparent irreversible amplification
- Apparent amplification resulted in the apparent residual sample strain

The effects of the temperature in the testing system on the measurements of thermal rock strain with clip-on extensometers

Abstract

The present work was aimed to identify and quantify the offsets biasing the thermal rock strain as measured with clip-on extensometers at a mechanical testing system (MTS) so as to increase the reliability of such measured strain. We conducted an experiment via cycling the temperature of a sample of aluminum alloy between ambient temperature and 90 °C under the hydrostatic confining pressure as maintained at 2 MPa. Thereby, the readouts of the extensometers appeared to be irreversible subsequent to the temperature cycle mimicking residual deformation in the sample. The numerically simulated temperature in the setup of the testing system was heterogeneous throughout such temperature cycling test showing an irreversible plug-in temperature in particular. These temperatures resulted in the apparent amplification of the circuit as constituted by the extensometer and the amplifiers as well as the relevant reading offset. Such induced offset biased the actual sample strain besides the expansion (contraction) in the metal parts of the extensometers yielding the apparent irreversible strain in the sample. We presented a workflow for quantifying the amplification- and the metal part-related offsets. The validity of the workflow was demonstrated via rectifying the strain in a rock sample that was monitored throughout a temperature cycle between 30 °C and 40 °C. Our present work would be referable for experimental researches on thermal rock strain with similar setup of measurement. The amplification- and the metal part-related offsets could be likewise estimated and excluded from the measurements conducted elsewhere before the strain in a tested sample could be obtained.

Keywords: Thermal rock strain; Plug-in temperature; Extensometers; Apparent amplification; Bankkalke; Temperature cycling test

1. Introduction

Sustainable utilization of geological subsurface reservoirs raises the needs for predicting the constitutive behavior and establishing the failure criteria of reservoir rocks in response to the change in temperature. The exploitation of geothermal energy would result in the decrease in temperature of the reservoir rock in the vicinity of the injection well [1]. The injection of carbon dioxide into the subsurface would cool down the casing material as well as the reservoir rock close to the flow conduit of the injected medium as the medium expands in an isenthalpic way [2]. Monitoring rock strain in a non-isothermal process e.g., a heating (cooling) ramp enables evaluating the expansivity of the rock per unit change in temperature. This evaluation permits assessing the effect of cooling on the potential of injection-induced seismicity [3] relevant to the zero horizontal strain boundary condition of the geological reservoir [4] and the decreased stress normal to the surfaces of existing faults. The analyses of rock inelasticity by the end of a conducted temperature cycle assist in identifying the constitutive relations governing the strain in reservoir rocks towards the change in temperature. Measuring the variation in fracture aperture of fractured rock samples upon the change in temperature [5, 6] allows prognosing the development of the fracture transmissivity for geofluids.

Besides the techniques that can be used to detect the changes in rocks' microstructure towards the variations in temperature [7-9], strain gauges and clip-on extensometers could also be used to measure the rock strain on a sample scale (10 cm). The clip-on extensometers based on resistive strain gauges are often applied monitoring thermal rock strain within the triaxial cell of a mechanical testing system (MTS). This application reduces the time as consumed by sample preparation and

increases the reproducibility of measurements, as compared to the case where strain gauges are directly affixed to a new sample before each individual experiment. On another aspect, the predetermined conditions of sample temperature could be better achieved within the cell in contrast to the application of digital image correlation methods with the cell open [10, 11]. In the latter case the heat transition into the surroundings raises challenges against sustaining the defined temperature in a sample. Furthermore, the thermal rock strain as monitored under predetermined triaxial stress states in the cell would be of more relevance to the practice of geological reservoir utilization. In comparison, the image correlation methods are mostly applied under unstressed and uniaxially stressed conditions.

In the present work, the thermal strain in the samples of aluminum alloy and limestone under cyclic temperature changes was measured using clip-on extensometers. Nevertheless, the readings of the extensometers in these tests were shown to be irreversible subsequent to the temperature cycles, respectively, mimicking residual sample strain. Such irreversible readings would hinder one from judging whether any deformational mechanisms had resulted in the apparent sample inelasticity throughout the temperature cycles.

In a study measuring deformation in electronic assemblies with strain gauges [12], it was claimed that an apparent strain was comprised in the gauge readings besides the gauge strain and the strain in the tested article. Such apparent strain was quantified using a function relevant to the magnitudes of the temperature as applied to the testing environment, although the origin of this strain was not clarified. In the measurements of forces and moments in wind tunnel tests using strain gauge balances, the influences on the measurements by the thermal gradients in the balances were evidenced [13-15]. The overall output of these strain gauge balances was shown to be reversible when the temperature in the balances was recovered. Nevertheless, the segments of the output-temperature curves relevant to the build-up and the reduction

of the thermal gradients exhibited significant hysteresis. Hence, it's presumable that the apparent strain having developed in the measurements with the strain gauge balances hinged upon not only the magnitudes of temperature but also the evolution of the temperature field in these balances. In another study monitoring soil structure deformation [16], the analysis on the apparent strain was extended correlating the readings of strain gauges to the average temperature in the environment, in which the circuitry of the gauges was located. For the measurement of thermal sample strain with extensometers in the present or similar testing system, the apparent strain associated with the deformation in the structural parts of the extensometers was recognized [17, 18]. Moreover, the offsets in sample strain relevant to the apparent wire temperature in the circuitry of the extensometers was also identified in [19]. However, this reported work neglected the influences on the apparent wire temperature by the heterogeneous temperature field in the testing system and the development of the field. Therefore, the reported work [19] was not referrable for elucidating the present evidenced recovery deficits in the output of the extensometers.

In the present study, we simulated the temperature as distributed in the applied mechanical testing system throughout the conducted temperature cycling tests, and compared the simulations to the monitored values. Thereby, the effect on the measurements with the extensometers by such temperature in the testing system was clarified. In particular, the plug-in temperature T_p would account for the present monitored irreversible readings of the extensometers. The plug-in temperature T_p represents the temperature at the plugs, through which the wires in the functioning circuitry of each extensometer are led into the triaxial cell of the testing system (see e.g., the point S in Fig. 1). We then presented an improved workflow for quantifying and eliminating the amplification- and the metal part-related offsets biasing the thermal sample strain. The validity of this workflow was supported by the consistency of the so rectified thermal rock strain per unit temperature to the reference values.

2. Testing equipment and procedures

2.1. Setup of testing equipment

The mechanical testing system (MTS 815 by MTS) applied in this study was constituted by the loading and the heating devices as well as the instruments detecting sample strain and temperature (Fig. 1). Hydraulic oil is pressurized by a primary pump operating at temperatures ranging from 40 °C to 75 °C. The operation temperature in this pump is sustained below the upper bound by an equipped water circulation cooling system, and is displayed at the panel of a built-in thermometer. Such pressurized hydraulic oil is led into the triaxial apparatus through a servo-controlled valve and propel the loading piston beneath the triaxial cell applying vertical stress. In another direction the hydraulic oil is led into a cylindrical confining pressure intensifier further pressurizing the silicone oil and applying confining pressure in the triaxial cell. The temperature in the cell can be cycled between 30 °C and predetermined magnitudes of up to 200 °C by operating the external thermal resistor-based heating devices. This temperature can be detected by up to 3 K-type thermocouples that are equipped in the cell. The coating made of glass wool is used insulating the cell in heating processes, and can be (partly) open so as to facilitate the ventilation using additional ventilators when the cell is being cooled down. Syringe pumps are also equipped for saturating the voids in the samples with fluid and pressurizing the pore fluid. The sample as prepared in a cylinder of 50 mm in diameter and 100 mm in length is mounted in the cell with the extensometers clipped on. Two axial extensometers labelled A and B (Model 632.90F) monitor the changes in half of the sample length, and a circumferential one labelled C (Model 632.92F) detects the variation in the sample perimeter, respectively. These extensometers can operate at temperatures up to 200 °C and at confining pressure up to 70 MPa. They enable measurements of displacement from -2.5 mm to 8 mm and from -4 mm to 7mm in the circumferential and

the axial sample directions, respectively, with a precision of ± 1 μm and an accuracy of 0.01% [20]. The working mechanism of the extensometers is briefly introduced in Appendix A (Fig. A.1).

2.2. Temperature cycling test on aluminum alloy

A temperature cycling test was implemented on a cylindrical solid sample of aluminum alloy (7075) of known thermal expansivity (≈23.2 με °C^{-1}) in an attempt to observe any offsets biasing the thermal sample strain. A hydrostatic confining pressure of 2 MPa was firstly applied to the sample-extensometer setup and sustained. When the readings of the extensometers upon this loading step became constant, the cell temperature T_c was cycled between 30 °C and 90 °C. Along the temperature cycle (Fig. 2a), isothermal stages were differentiated from the foregoing heating and cooling ramps, respectively, at the time instants when the calculated variation rates of cell temperature were below ± 0.1 °C h^{-1}. These isothermal stages, in which the cell temperature was apparently constant, were allowed for so as to distinguish any drifting in the measurements. The apparent plug-in temperature was measured using an infrared thermometer with a precision of 0.1 °C at the onset and the end of the heating ramp, at the outset of the cooling ramp and by the end of the temperature cycle, respectively. The average of three measurements at each studied time instant was evaluated. An annual average temperature of 30 °C in the laboratory was adopted to represent the ambient temperature T_a in this test.

The aluminum alloy (7075) was selected as the sample material due to the fact that the Young's modulus of the material, which amounted to 73 GPa at 30 °C, would only decrease 3.5% up to 90 °C [21]. Such induced compaction in the sample under the sustained confining pressure would only offset the readings of the extensometers by up to 10^{-1} μm, which would be out of the precision of the present extensometers (± 1 μm). We constrained the present temperature cycle up to 90 °C, in order to keep

the analyses on the strain offsets referable for the other experiments as conducted at the same temperature by the same testing system [e.g., [20]].

2.3. Temperature cycling test on rock sample

A second temperature cycling test was conducted on a sample of limestone (Neuburger Bankkalke) being an outcrop analog to the Malm formation in the Molasse basin, Germany [22]. This test was planned aiming to observe the similarity of the offsets in sample strain to those that could arise in the temperature cycle on the aluminum alloy. The oven-dried sample as sleeved with heat-shrink tubing was at first heated up to a temperature above the one that would be attained in the following temperature cycle (40 °C). It was so to constrain any extensive shrinkage in the tubing that would bias the sample strain throughout the temperature cycle. The sample was thereafter mounted up in the triaxial cell with the extensometers clipped on, before being vacuumed and then saturated at a hydrostatic confining pressure of 2 MPa following the procedures as depicted in [20]. When the strain in the sample due to the hydrostatic loading and saturation remained constant, we cycled the cell temperature T_c between 30 °C and 40 °C. The hydrostatic confining pressure and the pore pressure were kept at 2 MPa and 0.5 MPa throughout the temperature cycle, respectively. The cooling ramp in the implemented temperature cycle (Fig. 2b) took 72 hours due to the low differential temperature between the cell and the surroundings. The ambient temperature T_a in the laboratory was detected with a PT100 sensor and logged every five seconds in this test. The apparent plug-in temperature was likewise monitored at the aforementioned time instants.

We selected the Neuburger Bankkalke limestone as the sample also in an effort to quantify the thermal strain in the rock and keep the findings of the study referrable for the operation of the doublet hydrothermal system in the Molasse Basin [23]. Moreover, thermal cracking due to the differential expansivity of various mineral compositions would be constrained, as the present sample material is highly

homogeneous in terms of mineral content (>99% calcite). In addition, the hydrostatic confining pressure that could induce pore collapse in the Neuburger Bankkalke limestone was above 60 MPa [20]. The temperature and the heating rate that could result in thermal cracking in limestone would be above 200 °C and 120 °C h^{-1} [24, 25], respectively. Thus, the present sustained confining pressure of 2 MPa, the attained cell temperature of 40 °C as well as the heating (cooling) rates lower than $\pm$2.5 °C h^{-1} could well constrain the sample inelasticity and the relevant time-dependent strain. It would otherwise hinder one from identifying the reading offsets of the extensometers if such time-dependent sample strain would develop. Additionally, heating the limestone sample only up to 40 °C also made it possible to evaluate the temperature dependence of the strain offsets when the offsets would be compared to the ones that could arise in the test on the aluminum alloy.

Not least, the numerical simulation suggested that it took approximately up to 20 hours for the sample temperature to reach equilibrium (see Section 4.2). Thus, the present cycles of cell temperature were planned in the way allowing for full expansion (contraction) in the samples during the heating (cooling) ramps. It was in an effort to exclude such expansion (contraction) from the signals of the extensometers as monitored in the apparent equilibrium stage of cell temperature. In addition, up to 35.8 hours was allowed for these equilibrium stages in an attempt to observe whether the drifting in the readouts would eventually cease.

3. Numerical model setup

The setup of the present mechanical testing system was modelled using the Multiphysics simulator COMSOL following the finite element (FE) algorithm. The modelling was conducted in order to evaluate the heterogeneous temperature as distributed in the system during the present experiments. The 2-D model of the testing system was constituted by four domains of different materials. The domains included

the loading frame and the triaxial cell made of hardened steel, a sample of aluminum alloy (or limestone), the silicone oil in the triaxial cell and the hydraulic oil beneath the loading piston (Fig. B.1a; Appendix B). The temperature distribution in the system was simulated coupling the heat conduction [26] in the four domains as well as the heat transition into the surroundings via convection of air [27, 28].

To conduct the 2-D modelling, the average ambient temperature T_a was firstly assigned to the modelled experimental setup representing the initial temperature conditions therein. The heating path as implemented using the thermal resistor-based heating devices in each test was assigned to the contacts of these heaters to the outer lateral surface of the triaxial cell as a transient temperature boundary (B1; Fig. B.1a, b). The operation temperature of the primary pump in each test was applied as a constant temperature boundary (B2) at the contacts of the hydraulic oil to the steel parts in the experimental setup. This operation temperature was approximately at 75 °C and 50 °C in the tests on the samples of aluminum alloy and limestone, respectively. Four types of flux boundaries and a thermal contact were defined so as to model the heat transition from the experimental setup into the surroundings and from the base plate towards the bottom of the triaxial cell, respectively (Appendix B). Simulations were conducted using the 2-D model for the two temperature cycling tests, respectively. The simulated cell temperature $T_{c,s}$ in the wire end connecting to the strain gauges e.g., at the point Q and the plug-in temperature $T_{p,s}$ e.g., at the point S (Fig. 1) were applied in another 1-D model as depicted as follows.

The temperature in an extensometer differed from the one of the amplifiers in a temperature cycling test. Therefore, heat could conduct in the wires leading the strain gauges to the primary amplifier inducing a temperature therein (see Fig. A.1d). This induced temperature T_{ind} was additionally simulated using a 1-D line model (Fig. B.1c), as the diameter of the wire (<1mm) was considered to be negligible as compared to the wire length (8 m). The points Q, S as illustrated in Fig. 1 were located in this

line model at $x = -0.4$ m and $x = 0$ m, respectively. Another point U was located at $x = 7.6$ m denoting the wire end at the ambient temperature.

The average ambient temperature was firstly assigned to the line model representing the initial temperature condition therein. The cell temperature $T_{c,s}$ at the point Q and the plug-in temperature $T_{p,s}$ at the point S as derived from the above introduced 2-D modelling were then applied to the respective point in the line model as transient boundaries. In addition, the average ambient temperature was assigned to the point U as a concomitant constant boundary. The simulation using the line model was conducted for each extensometer in each of the present tests. The values of the material properties as applied in the modelling are listed in Table 1.

4. Results

4.1. Experimental results

The present monitored changes in sample dimensions being indicated by the readings of displacement at the extensometers are presented in Fig. 2. The readouts R_e of the extensometers comprised the initial readings of displacement D_{ini} and the thereafter measured displacements D_m.

In the temperature cycling test on the aluminum alloy, the displacements as monitored by the extensometers developed in an irreversible way, and manifested drifting under the attained isothermal conditions. The circumferential displacement increased 169 µm via heating up to 86 °C and showed afterwards a decrease of -205 µm until the outset of the cooling process (Fig. 2a). Thereafter, this signal sequentially decreased -265 µm in the cooling ramp down to 30 °C and -4 µm in the isothermal stage at 30 °C. The axial displacement as measured by the extensometer B showed an increase of approximately 11 µm up to 70.4 °C in the heating ramp and afterwards a decrease of -22 µm until the outset of the cooling process. Thereafter, this signal

decreased -24 μm in the cooling ramp and increased 4 μm in the isothermal stage at 30 °C, respectively. The axial extensometer A was out of operation in this test.

The expansion in the sample of a thermal expansivity of 23.2 με $°C^{-1}$ should have yielded positive displacements of about 204 μm and 60 μm by 90 °C at the circumferential and the axial extensometers, respectively. These displacements should have remained constant during the equilibrium stage at 90 °C and fully recovered by the end of the temperature cycle. However, these were not the case as reflected by the readings of the extensometers. Thus, the monitored displacements would comprise some offsets pertaining to the extensometers besides the expansion (contraction) in the sample.

In the temperature cycling test on the sample of limestone, the monitored displacements developed likewise in an irreversible way, and showed drifting under isothermal conditions. The circumferential displacement initially demonstrated a decrease of -3 μm as the cell temperature ramped up to 36 °C, and then manifested an increase of about 16 μm as the cell temperature attained 41 °C. Thereafter, this signal decreased -3 μm in the isothermal stage at 41 °C, then increased 2 μm in the cooling ramp down to 38.8 °C and finally decreased -13 μm by the end of the test (Fig. 2b). The readouts of the axial extensometer A showed a decrease of -4 μm in the heating ramp up to 40.5 °C, then demonstrated an increase of 1 μm in the subsequent isothermal stage and finally manifested an increase of 5 μm in the cooling ramp. In contrast, the displacement as monitored by the axial extensometer B decreased -3 μm upon heating to 40.5 °C, then increased 2 μm as the cell temperature was sustained in equilibrium and increased 4 μm in the cooling ramp eventually.

The thermal expansivity of limestone ranges from 1 με $°C^{-1}$ to 10 με $°C^{-1}$ [29]. The expansion in the sample should have yielded positive displacements up to 16 μm and 5 μm by 40 °C in the circumferential and the axial sample directions, respectively. These displacements should have not varied under the isothermal conditions and

should have been recoverable subsequent to the temperature cycle. However, the monitored displacements differed from these estimations in terms of the magnitudes, the direction of development and the residual readings. Thus, the present monitored values should also comprise the extensometer-related reading offsets. Moreover, the sample inelasticity had been well constrained by the predetermined test conditions (see Section 2.3). Hence, the monitored drifting in displacements was considered not to be relevant to any time-dependent sample strain due to inelasticity.

4.2. Numerical simulation

The simulated temperature distribution in the triaxial cell at specified time instants in the present tests was demonstrated in temperature isotherms, which showed apparent heterogeneity (Fig. B.2; Appendix B). Therein, the temperatures $T_{c,s}$ at the points O, P within the cell (see Fig. 1) cycled between 30 °C up to 93 °C in the test on the aluminum alloy and cycled up to 41 °C in the test on the limestone, respectively (Fig. 3a, b). The temperature at the point O, which was positioned horizontally 15 cm apart from the heating devices, was up to 9 °C higher than the value at the point P as located 21 cm apart from the heating devices (Fig. 3a). The deficits of the simulations to the values $T_{c,m}$ as measured using the thermal couples were of magnitudes below 3% of the measurements. The simulated temperature $T_{c,s}$ in the wire end connecting to e.g., the circumferential extensometer (point Q, Fig. 1) cycled up to 88 °C and 40 °C in the respective test (Fig. 3a, b). In contrast, the simulated plug-in temperature $T_{p,s}$ of the same extensometer (point S) developed in an irreversible way. In particular, this temperature remained at 54 °C and 34 °C by the end of respective experiment, appearing to be above its initial value of about 30 °C. The simulations of the plug-in temperature were in consistency to the values as measured with the infrared thermometer at specified time instants. In addition, the plug-in temperature varied up to 1.4 hours and 1.7 hours prior to the temperatures at the

extensometer (point Q) and in the center of the sample in the respective experiment (Fig. 3c, d).

The simulated temperature in the aluminum alloy attained nominal equilibrium at 86 °C in about 13.9 hours from the onset of the temperature cycle. In this nominal equilibrium, the sample temperature decreased from 86.2 °C in the bottom to 85.2 °C in the top showing an average thermal gradient of -0.1 °C cm^{-1}. In the cooling process, it took approximately 22 hours for the sample temperature to be fully recovered to 30 °C. In the case of the limestone, the simulated sample temperature attained nominal equilibrium at 40 °C in about 14.7 hours from the outset of the experiment. In this nominal equilibrium, the sample temperature decreased from 41.4 °C in the bottom to 39 °C in the top presenting an average thermal gradient of -0.24 °C cm^{-1}. Nevertheless, the temperature along the sample radius only showed differences below -10^{-2} °C cm^{-1} towards the sample center in the both experiments.

The temperature as induced in the wire (Fig. B.1c) is exemplified using the 1-D modelling results by the axial extensometer B throughout the test on the aluminum alloy (Fig. 4a). This induced temperature T_{ind} varied with the positions L along the length of the wire. Moreover, the manner in which this temperature distributed developed as time proceeded. For example, at the outset of the cooling ramp (t_3), the temperature T_{ind} up to 89 °C showed approximately linear distribution in both the in-cell and the out-cell wire segments. By the end of the test (t_4), T_{ind} remained between 31 °C and 54 °C due to the concurrent plug-in temperature at $x = 0$ m, although the in-cell and the out-cell wire ends had been cooled down to about 31 °C.

In short summary, the cycling of the temperature in the triaxial cell was primarily controlled by the heating paths as implemented at the heating devices (Fig. B.1b). In the equilibrium of the measured cell temperature, an average thermal gradient of -1.3 °C cm^{-1} was manifested in the silicone oil from the inner wall of the cell towards the sample. The concomitant axial and radial thermal gradients in the samples were

apparently lower than the one in the silicone oil as the sample materials were more conductive than the oil in terms of heat (Table 1). Thereby, the concurrent sample temperature was considered to be in equilibrium. Additionally, the irreversible development of the plug-in temperature and the wire temperature was mainly due to the effect of the operation temperature of the primary pump. The comparability of the simulated cell temperature and plug-in temperature to the measurements using the thermal couples and the infrared thermometer, respectively, would validate the present 2-D modelling. The base plate, in which the plug-in temperature was measured, was heated up not only by the heating devices but also by the hydraulic oil at the operation temperature of the primary pump. However, the samples and the extensometers were heated up mainly by the heating devices via the silicone oil. Thus, the plug-in temperature developed preceding the temperatures at the extensometers and in the samples. It would be presumable that the different parts in the testing system could respond to the variation in temperature asynchronously in an individual test.

5. Workflow for correcting thermal rock strain

A previous study [19] revealed the effect of the induced temperature T_{ind} in the wire between the strain gauges and the primary amplifier on the wire resistance. This apparent wire resistance would yield a primary amplification factor A'_p differing from the value at the reference temperature. Such apparent factor biased the changes in the sample dimensions besides the offsets related to the expansion (contraction) in the metal chips on which the strain gauges were fixed. In this reported work, however, the amplification- and the metal chip-related reading offsets were evaluated using the average of the cell temperature as measured by two thermal couples. This evaluation did not account for the heterogeneity and the asynchronous development of the temperature in different positions in the testing system neither the relevant effects on the measurements.

Hence, in the following, we evaluate the aforementioned offsets in an improved way. Particularly, the irreversible character of the plug-in temperature is incorporated in the estimation of the amplification-related offsets. Moreover, the localized cell temperature at each extensometer is taken into account for estimating the metal chip-related offsets. Thereby, the application of the workflow for rectifying thermal rock strain is demonstrated.

5.1. Amplification-related offsets

The apparent primary amplification factor A_p' as developed throughout a temperature cycle was estimated as following $A_p' = R_v'/(R_{in}' + R_{out}')$. R_{in}', R_{out}', R_v' denote sequentially the apparent resistances of the in-cell and the out-cell wire segments and the rheostat. The apparent resistance of the in-cell wire segment read $R_{in}' = R_{in}(1 + \gamma dT_{ind,i})$. Therein, $\gamma dT_{ind,i}$ represents the relative increase in the initial resistance R_{in}. Such relative increment is addressed by the fractional increase in wire resistance per unit temperature γ [30] and the change in the in-cell wire temperature $dT_{ind,i}$ referring to 30 °C. At any time instant of interest, the temperature $T_{ind,i}$ varied with the positions L along the wire length l_{in} (Fig. 4a). Thus, the concurrent wire resistance R_{in}' was derived by: (1) calculating the apparent resistance per unit wire length $R_{in}^* = R_{in}(1 + \gamma dT_{ind,i})/l_{in}$ and (2) integrating the R_{in}^*-L function over the wire length. The apparent wire resistance R_{in}' at other studied time instants was obtained by repeating the steps (1), (2) (see Fig. 4b).

The apparent resistance of the out-cell wire piece could be formulated in $R_{out}' = R_{out}(1 + \gamma dT_{ind,o})$ and quantified likewise as for estimating the in-cell counterpart. Here $dT_{ind,o}$ denotes the change in the out-cell wire temperature referring to 30 °C. Not least, no temperature-related effect of the rheostat had been evidenced influencing the readouts of the extensometers in the present study. Hence, the apparent resistance of the rheostat R_v' was considered to be equivalent to its initial

value R_v (see Table A.1). Thereby, the apparent primary amplification factor could eventually be obtained as following $A'_p = R_v/(R'_{in} + R'_{out})$. The amplification-related offsets D_{amp} into the readouts of the extensometers R_e could then be formulated in $D_{amp} = R_e\left(1 - A_p/A'_p\right)$.

In the previous study [19], the averaged cell temperature was used to represent the apparent in-cell wire temperature $T_{ind,i}$, and was applied as the only transient boundary for modelling the induced out-cell wire temperature. However, this average addressed neither the influence of the heterogeneous cell temperature on the in-cell wire piece (Fig. B.2) nor the effect of the irreversible plug-in temperature on the overall wire temperature (Fig. 4a). In comparison, it would be more reasonable to evaluate the temperature in both the in-cell and the out-cell wire pieces as in the present numerical modelling including the plug-in temperature as a transient boundary also.

As exemplified in Fig. 4b, the apparent resistances of both the in-cell (R'_{in}) and the out cell (R'_{out}) wire pieces increased in the heating ramp of the temperature cycle on the aluminum alloy. This resulted in the concomitantly decreasing apparent amplification A'_p. The further increase in the out-cell wire resistance R'_{out} in the equilibrium stage at 90 °C gave rise to the concurrent time-dependent decrease in the amplification A'_p. Afterwards, the wire resistances R'_{in}, R'_{out} were partly recovered until the end of the temperature cycle due to the remaining apparent wire temperature (Fig. 4a), leaving the recovery deficit in the amplification A'_p.

The development of the amplification-related offsets D_{amp} complied with the evolution of the apparent amplification A'_p as well as the wire resistances R'_{in}, R'_{out}. Such offsets D_{amp} displayed increasing magnitudes in the heating processes as well as the drifting at the sustained temperatures, and partly remained by the end of the temperature cycles (Fig. 5). Moreover, the magnitudes of the offsets D_{amp} also showed dependence upon the temperature in the testing system. It developed up to

40 µm at 40 °C and up to 460 µm at 90 °C by the extensometer C, while evolved up to 3 µm at 40 °C and up to 120 µm at 90 °C by the extensometers A, B.

5.2. Metal part-related offsets

Upon expansion (contraction), the metal chips also biased the variation in the sample dimensions in addition to the amplification-related offsets [19]. In order to rectify the thermal rock strain as developed under defined temperature conditions, it is necessary to evaluate the metal chip-related offset D_{mte} and its dependence on temperature. We obtained such offset D_{mte} via excluding the amplification-related offsets D_{amp} and the changes in sample dimensions D_A from the overall displacements D_m as monitored in the temperature cycle on the aluminum alloy. Thereby, the offset D_{mte} reads $D_{mte} = D_m - D_{amp} - D_A$.

The variation in the circumference of the aluminum alloy $D_{A,c}$ upon thermal expansion (contraction) was formulated in $D_{A,c} = 2\pi r_0 \alpha_A d\overline{T_A}$. Here, r_0, α_A denote, respectively, the reference sample radius and the temperature-dependent thermal expansivity of the alloy (7075) referring to the sample dimension at 30 °C. $d\overline{T_A}$ represents the increment in the average temperature along the sample radius at the middle height of the sample referring to the initial temperature of 30 °C. Similarly, the axial extension (shortening) in the sample $D_{A,l}$ was estimated as referred to half of the sample length $l_0/2$ following $D_{A,l} = l_0 \alpha_A d\overline{T_A'}/2$. Therein, $d\overline{T_A'}$ denotes the change in the average temperature in the sample's lateral surface as confined by the pair of metal cones in the axial extensometer. The sample would have been compacted due to the sustained confining pressure and the reduced Young's modulus during heating (Section 2.2). The so induced dimensional changes of the aluminum alloy would be -0.11 µm and -0.04 µm in the circumferential and the axial sample directions, respectively. Hence, the extension in the sample circumference $D_{A,c}$ and the length $D_{A,l}$ referring to the sample dimensions at 30°C would be overestimated by 1×10^{-4}

μm and 3×10^{-5} μm, respectively. These overestimates, however, appeared to be negligible as compared to the dimensional changes of the sample due to expansion (Table 2).

The obtained metal chip-related offsets D_{mte} appeared to be reversible by the end of the temperature cycle (Fig. 5a). Such offsets D_{mte} amounted to 0.84 μm as well as 4 μm per degree by the axial (B) and circumferential (C) extensometers, respectively, when averaged over a change in temperature of ±58 °C in the metal chips. The temperature in a metal chip was evaluated using the simulated value at the point in the triaxial cell where the respective extensometer was positioned.

In short summary, the amplification- and the metal chip-related offsets as well as the dimensional changes of the aluminum alloy constituted the measured displacements (Table 2). However, the time-dependent drifting and the recovery deficits in the monitored displacements were attributed to the amplification-related offsets only. In comparison, the magnitudes of the reading offsets amounted up to 1.9 times of the axial extension in the sample and up to 2.3 times of the increase in the sample circumference, respectively. The present estimation of the changes in sample dimensions and the derivation of the metal chip-related offsets would address the asynchronous development of the heterogeneous temperature in the cell. Such evaluation would be of advantage over the one in the previous study [19]. Therein, the deformation in the sample and the metal chip was estimated respectively with the same averaged cell temperature, as if they had responded to the changes in temperature simultaneously.

It is noticed that the axial displacement as monitored at the sample of aluminum alloy developed in a way opposite to the measurements in the axial direction of the limestone sample (Fig. 2). This phenomenon was attributed to the initial directions in which the metal cones were displaced and the metal chips were incurvated, respectively, when the axial extensometers were clipped on the samples [19]. It is

assumed that a metal chip would be of equivalent expansivity to the change in temperature in the both cases when it bulged towards or backwards the metal cones. Hence, we evaluated the metal chip-related offsets using -0.84 µm °C^{-1} for the measurement on the limestone with the axial extensometers.

5.3. Corrected thermal rock strain

We rectified the variations in the dimensions of the limestone sample D_r via eliminating the amplification- and the metal chip-related offsets sequentially from the monitored displacements (Fig. 5b). The metal chip-related offsets were estimated so that the expansion (contraction) in the chips per unit temperature was multiplied to the increment in the temperature of the chips.

The rectified increases in the circumference and the length of the limestone sample amounted up to 7 µm and 2 µm, respectively, and were shown to be reversible throughout the temperature cycle. However, the measured displacements mimicked an irreversible shortening of -3 µm in the sample circumference and a residual extension of 2.5 µm in the sample length by the end the of test, respectively (Fig. 5b). The drifting and the residuals in the measured displacements were relevant to the amplification-related offsets only. The magnitudes of the reading offsets amounted up to 4.5 times of the increase in the sample length and up to 5.9 times of the increase in the sample circumference, respectively (Table 2).

The axial sample strain ε_a was evaluated by referring the rectified change in sample length to the original distance of 50 mm between the two metal cones of each axial extensometer. The lateral (radial) sample strain ε_l was determined by calculating the change in the sample radius using the rectified variation in the perimeter and referring this change to the original radius. The so derived axial and lateral strain in the tested limestone amounted up to -40 µε, -41 µε and -48 µε by 40 °C, respectively (Fig. 6a). Such strain was notated negative representing the extension in

the sample length and radius [31]. The thermal expansivity of the present tested limestone amounted to 4.3 με °C^{-1}, which was approximated via averaging the above derived strain to a change in temperature of 10 °C. This approximation showed consistency to the reference values of the Veselje Unito limestone (4.1 με °C^{-1} to 4.8 με °C^{-1}) and the Mannersdorfer limestone (4.0 με °C^{-1} to 4.5 με °C^{-1}) [32] with deficits ranging from -10% to 5% and from -4% to 8%, respectively. In this reference work [32], the aforementioned limestones were tested in temperature cycles between ambient temperature and 80 °C, of which the changes in dimensions were monitored with LVDTs. Therein, the offsets in the rock strain as induced by the LVDTs was quantified via conducting the same temperature cycles on a dummy sample of known thermal expansivity. The LVDT-related offsets were then excluded from the measurements on the limestones for correcting the rock strain. The deficits of the present rectified thermal expansivity to the reference values would be attributed to the heterogeneity of the different limestone samples. Furthermore, the present approximated thermal expansivity was accordant with the estimates between 4.1 με °C^{-1} and 4.3 με °C^{-1} showing differences up to 5%. These estimates were made following a model [33], which treated the present sample as an integrity of the rock solids and the water in the rock voids. The deformational moduli [34-36] and the thermal expansivity [37, 38] of the both constituents were addressed in the model.

The variation in the sample volume was represented using the corrected volumetric strain ε_v, which was formulated in $\varepsilon_v = 2\varepsilon_l + \bar{\varepsilon}_a$ including the average of the rectified axial strain $\bar{\varepsilon}_a$. Such corrected volumetric strain ε_v, being notated negative, showed expansion of down to -137 με by 40 °C. This expansion appeared to be reversible by the end of the temperature cycle (Fig. 6b). Nevertheless, the namely monitored volumetric strain ε_v', which was computed with the monitored displacements, fluctuated substantially obscuring the behavior of the sample (Fig. 6c). Along the heating ramp attaining 36.5 °C, the increased amplification-related strain offsets

$\varepsilon'_{v,amp}$ = 200 με exceeded its counterpart pertaining to the metal chip $\varepsilon'_{v,mte}$ = -90 με and the corrected rock strain ε_v = -30 με (Fig. 6b). This gave rise to the concurrent overall compaction in the monitored strain and the peak value of ε'_v = 80 με at 36.5 °C (Fig. 6c). In the subsequent heating process up to 40 °C, the dilation in the metal chip and the sample accumulated and gradually exceeded the amplification-related strain offset $\varepsilon'_{v,amp}$. Hence, the concomitant monitored strain ε'_v developed retrogradely to lower values. In the following isothermal stage, the amplification-related strain offsets $\varepsilon'_{v,amp}$ developed alone, accounting for the time-dependent compaction as shown by the monitored strain ε'_v. Along the cooling ramp down to 36.8 °C, the decrease in the strain offsets $\varepsilon'_{v,amp}$ = -200 με outstripped the increase in the other offsets $\varepsilon'_{v,mte}$ = 100 με and the sample strain ε_v = 30 με. Thereby, the concurrent monitored strain ε'_v manifested overall dilation and the trough value at 36.8 °C. In the following cooling process, the contraction in the sample and the metal chip gradually dominated the monitored strain yielding overall contraction.

The workflow for rectifying the thermal strain in the limestone sample is summarized in Fig. 7. The comparability of the rectified thermal expansivity of the limestone to the reference values would validate such workflow. The interplay amongst the rectified sample strain and the strain offsets resulted in the development of the monitored apparent sample strain.

6. Discussions

6.1. The effect of plug-in temperature

The heating path (time)-dependence of the apparent amplification was addressed in the preliminary work [19] by correlating the development of the amplification to the monitored cell temperature rather than to the plug-in temperature. It was so as the reported study was conducted based on experimental observations

following a heating plan that ended up in an isothermal step at 60 °C. Thereby, no irreversible displacement was monitored and accordingly no attention had been drawn to the heterogeneous temperature as distributed in the testing system, more specifically, the plug-in temperature. Nevertheless, the irreversible development of the plug-in temperature could result in the recovery deficits in the apparent wire temperature and the amplification-related offsets (Figs. 4, 5). If the reported work had been repeated for analyzing the present measurements, it would have led to such primary amplification factors A_p^* that developed in a reversible manner (see Fig. 4b). Moreover, the thereby assumed homogeneous temperature in the in-cell wire segment would thus have been represented using the average of the measured cell temperature $T_{c,m}$. Such averaged cell temperature could have delivered underestimated apparent amplification upon heating and the overestimates upon cooling as following $A_p' = R_v/\left[R_{in}\left(1+\gamma dT_{c,m}\right)+R_{out}\left(1+\gamma dT_{ind,o}\right)\right]$. Consequently, the apparent irreversible deformation in the aluminum alloy as observed subsequent to the present temperature cycle could have not been clarified. Moreover, the estimates of the amplification-related offsets would have been biased.

The present simulated heterogeneous wire temperature T_{ind} at each studied time instant could be equilibrated using an assumed equivalent temperature T_{eq}. The equivalent temperature T_{eq} was defined so that the apparent wire resistance related to this temperature T_{eq} equals the one due to the heterogeneous temperature T_{ind} in the wire. Hence, the temperature T_{eq} at any studied time instants could be obtained via solving $(R_{in}+R_{out})\left(1+\gamma dT_{eq}\right)=R_{in}\left(1+\gamma dT_{ind,i}\right)+R_{out}\left(1+\gamma dT_{ind,o}\right)$. The increments of temperatures as included in this equation were referred to the initial temperature in the wire. As observed in the exemplary case of the limestone, the magnitudes of the amplification-related offsets D_{amp} developed in a way strongly dependent on the evolution of the equivalent temperature T_{eq} (see TC_1, Fig. 8a).

Such D_{amp}-T_{eq} dependence could be depicted using the slopes of the fitted linear curves amounting up to 4.3 µm °C^{-1} (Fig. 8b).

Another equivalent temperature T'_{eq} was also calculated for the alternative case. In this case, the average of the measured cell temperature, instead of the plug-in temperature, had been applied as a transient boundary for simulating the induced wire temperature T_{ind}. Such equivalent temperature T'_{eq} was shown to be reversible due to the cycled cell temperature (TC_1, Fig. 8a). The temperature T'_{eq} would perhaps account for the amplification-related offsets D_{amp} developing up to the onset of the cooling ramp. However, it could not address the offsets D_{amp} that were only partly removed in the cooling process. Moreover, the heating and cooling segments of the D_{amp}-T'_{eq} curves showed apparent hysteresis (Fig. 8c).

In the case the temperature cycle as conducted on the limestone (Fig. 2b) had been repeated once consecutively, we also derived the equivalent temperatures T_{eq}, T'_{eq} via numerical modelling (TC_2, Fig. 8a). The amplification-related offsets D_{amp} could then be estimated as following $D_{amp} = (D_{ini} + D_{mte} + D_r)\left(1 - A_p/A'_p\right)A'_p/A_p$. Thereby, the initial readings D_{ini} at the outset of the conducted temperature cycle (TC_1) was applied. The metal chip-related offsets D_{mte} and the dimensional changes of the limestone D_r were evaluated using the values as derived from this conducted cycle, respectively. Such estimated amplification-related offsets D_{amp} in the modelled temperature cycle (TC_2) showed consistent dependences on the equivalent temperature T_{eq} as in the conducted one (Fig. 8b). Moreover, it was shown that the hysteresis between the heating and cooling segments of the D_{amp}-T'_{eq} curves could develop in the modelled temperature cycle (Fig. 8c).

We presented the hysteresis amongst the D_{amp} - T'_{eq} curves so as to demonstrate the inaccuracy, which could be induced by neglecting the effect of the plug-in temperature when the wire temperature T_{ind} was simulated. In addition, we

were not aimed to deliver an individual value depicting the dependence of the amplification-related offsets D_{amp} on the equivalent temperature T_{eq}. Such dependence varied as the magnitude and the sign of the offsets D_{amp} also hinged upon the initial readings by mounting-up, the offsets pertaining to the metal chip and the expansivity of the tested sample material. However, the derivation of the equivalent temperatures T_{eq}, T'_{eq} as for the aforementioned occasions permitted clarifying the effect of the plug-in temperature on the amplification-related offsets and on the measured displacements.

6.2. Applicability of the workflow

The deviation in the primary amplification factor of the present clip-on extensometers from its calibrated value would be ineluctable in the measurements of thermal rock strain in a mechanical testing system (MTS). We evaluated the dependencies of such induced offsets in the measurements upon the heterogeneous temperature in the testing system and on the development of this temperature. The validity of the workflow for correcting such measured thermal strain would be supported by the consistency of the rectified rock strain per unit temperature to the reference values. The rectification, though constrained to 40 °C, would be applicable at the upper-bound operation temperature (200 °C) of the testing system. In particular, the primary amplification factor could have been reduced by 23% of its initial value during the equilibrium of cell temperature at 200 °C, and eventually remained at 95% of the initial value. These estimates were made assuming that the present temperature cycle on the limestone had been extended up to 200 °C whilst the primary pump had operated at its upper-bound temperature of 75 °C. The apparent shortening in the sample length was expected to be down by -110 μm, and the extension in the perimeter could be up to 870 μm, respectively. These estimates were derived via extrapolating the linear relation of the amplification-rectified displacements to the cell temperature as obtained from the present limestone-extensometer setup. Moreover, increases of

up to 59 µm in the sample length and an increase of 190 µm in the sample perimeter could be derived, respectively, via excluding the metal chip-related offsets D_{mte} from the above mentioned extrapolates. These offsets D_{mte} at 200 °C amounted to -167 µm and 680 µm at the axial and the circumferential extensometers, respectively. The rectified changes in the sample dimensions delivered an average thermal expansivity of 7 µε °C^{-1} up to 200 °C. This average thermal expansivity was accordant with the estimates between 6 µε °C^{-1} and 10 µε °C^{-1} as following the theoretical model [33].

Thermal cracking in limestones could be constrained by heating only up to 200 °C at heating rates below 120 °C h^{-1} (Section 2.3). The thereby developed sample deformation would be of an elastic feature being consistent with the rock strain as developed in the present temperature cycle up to 40 °C. Therefore, the above introduced extrapolation of the amplification-rectified displacements to 200 °C was considered to be valid. However, in temperature cycles on limestones exceeding 200 °C, the likely induced rock inelasticity upon thermal cracking would develop under the sustained confining pressure. Such developed rock inelasticity would deliver another time-dependent segment to the monitored rock strain. Then, the above suggested extrapolation does not apply. In addition, the heterogeneity in other rock samples e.g., the beddings in shale and the differential thermal expansivity of the minerals in granite could induce rock inelasticity upon the changes in temperature as well [7-9]. In the presence of induced rock inelasticity, the amplification- and the metal chip-related offsets should be excluded from the measurements before the actual thermal rock strain and its time-dependent development could be revealed.

The presented workflow for quantifying and eliminating strain offsets (Fig. 7) facilitates rock strain investigations following defined heating paths and loading paths. The rectified thermal rock strain upon cyclic temperature changes under a predetermined stress state would perhaps manifest a threshold temperature for inducing rock inelasticity. When the attained upper (lower)-bound temperature

exceeded this threshold, residuals in the rock strain would be evidenced subsequent to the temperature cycle. Analyzing the rectified strain-stress curves upon deviatoric loading under isothermal conditions at a series of defined temperatures permits identifying a critical temperature. Exceeding this temperature, the failure mode in the tested material could transfer from the brittle regime to the ductile one.

For the present extensometers, the apparent output potential V_{op} could be formulated in $V_{op} = 10A'_p\, A_s(\varepsilon_i - \varepsilon_b)/[2/K - (\varepsilon_b + \varepsilon_i)]$. This formulation takes into account the bridging of the strain gauges as fixed to each metal chip, the sensitivity factor K of each strain gauge and the apparent primary amplification A'_p. In addition, ε_b, ε_i represent the deformation in the strain gauges on the bulged side and the incurvated side of a metal chip, respectively. The coefficient 10 denotes the excitation potential as applied to the bridging of the strain gauges. As the gauges on the bulged chip side were extended and the counterparts on the incurvated side were shortened, the values of ε_b and ε_i should be of opposite signs. It is presumable that the strain in the extended gauges would be of equivalent magnitude to the strain in the shortened counterparts, i.e., $\varepsilon_i = -\varepsilon_b$. The output V_{op} could then be simplified into $V_{op} = 10A'_p\, A_s\varepsilon_i K$. The factor K is slightly temperature-dependent being of a relative increment of 0.01% °C^{-1} rather than a constant as evaluated at the reference temperature of 30 °C. The so induced error would account for up to 1.7% of the output V_{op} at 200 °C. Additionally, the fraction of such error in the output would be further reduced to 1.3% by the concomitant apparent primary amplification A'_p. Thus, the error in the measurements pertaining to the temperature-dependent sensitivity factor of the strain gauges could be neglected.

The pressurized silicone oil in the triaxial cell applied confining pressure on the both sides of the metal chip. The increasing confining pressure upon hydrostatic loading would also compact the strain gauges adhered on both sides of the chip

equivalently. This compaction would reduce the diameter and increase the length of the filamentary resistor of the gauges. Likewise, the sustained confining pressure would also compact the filamentary resistor at increasing temperature due to the decreasing deformational modulus of the resistor material. The thereby induced relative increases in the resistance of the four strain gauges would be equivalent. Thereby, the allocation of the excitation potential on the gauges or the output from the bridging of the gauges would not be changed. Hence, the effect on the measurements by the rheological behavior of the strain gauges pertaining to the confining pressure [39] could be neglected.

The simulated cell temperature $T_{c,s}$ at the wire end connecting to each extensometer and the plug-in temperature $T_{p,s}$ were applied as transient boundaries for modelling the in-cell wire temperature (see Figs. 1, B.1c). Due to the heterogeneity of the temperature in the triaxial cell (Fig. B.2), the in-cell wire would have crossed a few domains of different temperatures depending upon the shape of the wire and its position in the cell. Hence, the modelling using the aforementioned temperature boundaries of $T_{c,s}$ and $T_{p,s}$ only, would render the simulated wire temperature different from the real situation. Nevertheless, the shape and position of the in-cell wire of each extensometer would vary by mounting-up before each individual experiment, and were subjected to changes when the cell was being filled with silicone oil. Therefore, the present simulated in-cell wire temperature was applied to represent the situation in practice. This might be improved via preparing the in-cell wire in a suitable length so that the shape of the wire and its position in the cell could be kept almost the same in the tests. Thereby, the simulation of the in-cell wire temperature could be facilitated by applying the heterogeneous cell temperature as derived from the present 2-D modelling (Fig. B.2). In addition, the 1-D modelling did not address the heat transition from the wiring material through the insulation of the wires towards the surrounding environment. Furthermore, the actual wire temperature, temporarily, could

not be measured with the available thermometers. Assuming that this heat transition could be impeded by the insulation, we applied the simulated wire temperature to represent the actual values in the present study.

In future work, the 1-D modelling should be improved incorporating the heat conduction in the insulation and the convection at the insulation surfaces. Alternatively, the method for monitoring and logging the actual wire temperature as well as the plug-in temperature should be developed in order to improve the estimation of the apparent wire resistance. The feasibility of replacing the wiring material with the conductors of less sensitivity to the changes in temperature in terms of resistance could also be concerned in an effort to constrain the variations in the amplification. Not least, the apparent expansivity of the metal chips under the changes in temperature at the confining pressure above 2 MPa should be extensively investigated.

7. Conclusions

The present study identified and quantified the offsets biasing the thermal rock strain as measured with clip-on extensometers in a mechanical testing system (MTS). Temperature cycling tests as implemented on a reference sample of aluminum alloy and a limestone sample, respectively, manifested the offsets in the measurements. Numerical simulations as conducted in parallel revealed the effects of the heterogeneous temperature in the testing system and its development on the experimentally measured sample strain. The findings out of the present work are list as follows.

The monitored changes in the sample dimensions mimicked irreversible sample strain by the end of the temperature cycle in each test.

The simulated temperature in different positions within the testing system demonstrated heterogeneity as well as asynchronous development. The irreversible evolution of the plug-in temperature throughout the temperature cycles was revealed.

The plug-in temperature strongly influenced the wire temperature in the functioning circuitry of the extensometers and the wire resistance. The varied wire resistance yielded the irreversible apparent amplification and led to the monitored residual sample strain.

The amplification-related offsets were shown to be linearly relevant to the approximated equivalent wire temperature. The magnitudes of the amplification- and the metal chip-related strain offsets amounted up to 5.9 times of the rock strain, and increased with increasing temperature.

The validity of the workflow as proposed for rectifying the thermal rock strain was supported by the consistencies of the corrected thermal expansivity of the tested rock material to the literature values and the theoretical values. The deficits of the corrected value to the literature values and the theoretical values amounted from -10% to 8% and up to 5%, respectively.

Our work would be referable for other experiments in rock mechanics and material sciences investigating thermal strain in different (rock) materials at similar testing systems under predetermined temperature conditions. The work suggested that it would assist in identifying the origin of reading offsets of clip-on extensometers to investigate the temperature field in the practical environment where the extensometers are applied. Following the present study, the amplification- and the metal chip-related offsets could accordingly be quantified and eliminated for observing (time-dependent) thermal sample strain. The evaluation of such derived thermal strain permits studying the constitutive relation and the failure criteria of the tested material under the thermo-mechanical coupled conditions. Such strain would also reflect the

changes in the microstructure of the material and enable prognosing the relevant consequence on the material transmissivity for fluid.

Acknowledgements

We thank Liane Liebeskind for operating the mechanical testing system. This study was funded by the IMAGE-Project within the 7th Framework Program of the EU (Grant No.: 608553).

References

[1] M. Dussel, E. Lüschen, R. Thomas, T. Agemar, T. Fritzer, S. Sieblitz, B. Huber, J. Birner, R. Schulz, Forecast for thermal water use from Upper Jurassic carbonates in the Munich region (South German Molasse Basin), Geothermics 60 (2016) 13-30.

[2] Z. Fang, X. Li, Preliminary assessment of CO2 geological storage potential in Chongqing, China, Procedia Environ. Sci. 11C (2011) 1064-1071.

[3] G. Blöcher, M. Cacace, A.B. Jacquey, A. Zang, O. Heidbach, H. Hofmann, C. Kluge, G. Zimmermann, Evaluating micro-seismic events triggered by reservoir operations at the geothermal site of Groß Schönebeck (Germany), Rock Mech. Rock Eng. 51 (2018) 3265-3279.

[4] X. Hou, S. Liu, G. Li, Y. Zhu, A. Liu, Quantifying and modelling of in situ stress evolutions of coal reservoirs for Helium, methane, nitrogen and CO2 depletions, Rock Mech. Rock Eng. 54 (2021) 3701-3719.

[5] M.G. Lima, D. Vogler, L. Querci, C. Madonna, B. Hattendorf, M.O. Saar, X. Z. Kong, Thermally driven fracture aperture variation in naturally fractured granites. Geotherm. Energy 7(23) (2019). https://doi.org/10.1186/s40517-019-0140-9.

[6] H. Peng, Z. Zhao, W. Chen, Y. Chen, J. Fang, B. Li, Thermal effect on permeability in a single granite fracture: experiment and theoretical model, Int. J. Rock Mech. Min. Sci. 131 (2020) 104358.

[7] N.N. Sirdesai, A. Singh, L.K. Sharma, R. Singh, T.N. Singh, Determination of thermal damage in rock specimen using intelligent techniques, Eng. Geol. 239 (2018) 179-194.

[8] B. Mahanta, V. Vishal, N. Sirdesai, P.G. Ranjith, T.N. Singh, Progressive deformation and pore network attributes of sandstone at in-situ stress states using computed tomography, Eng. Fract. Mech. 252 (2021) 107833.

[9] V. Srinivasan, A. Tripathy, T. Gupta, T.N. Singh, An Investigation on the Influence of thermal damage on the physical, mechanical and acoustic behavior of Indian Gondwana shale, Rock Mech. Rock Eng. 53 (2020) 2865–2885.

[10] J. Song, J. Yang, F. Liu, K. Lu, High temperature strain measurement method by combining digital image correlation of laser speckle and improved RANSAC smoothing algorithm, Opt. Lasers Eng. 111 (2018) 8-18.

[11] L. Tian, L. Yu, B. Pan, Accuracy enhancement of a video extensometer by real-time error compensation, Opt. Lasers Eng. 110 (2018) 272-278.

[12] P. Hall, R. Deighan, On using strain gauges in electronic assemblies when temperature is not constant, T-CHMT 9 (1986) 492-497.

[13] J. Hereford, P.A. Parker, R.D. Rhew, Impact of thermal gradients on wind tunnel force measurements, in: 37th AIAA Aerospace Sciences Meeting and Exhibit, Nevada, 1999.

[14] K.C. Lynn, S.A. Commo, T.H. Johnson, P.A. Parker, Thermal and pressure characterization of a wind tunnel force balance using the single vector system, in: 49th AIAA Aerospace Sciences Meeting including the New Horizons Forum and Aerospace Exposition, Florida, 2011.

[15] C. Wang, P. Mi, Z. Tian, G. Yi, Study on temperature characteristics and correction of strain gauge balance in actual airflow environment, Aerosp. Sci. Technol. 106 (2020) 106201.

[16] C.L. Meehan, M. Talebi, A method for correcting field strain measurements to account for temperature effects, Geotext. Geomembr. 45 (2017) 250-260.

[17] X.Y. Hu, J.H. Jia, S.T. Tu, Displacement amplifier design for an extensometer in high temperature deformation monitoring, Procedia Eng. 29 (2012) 1872-1876.

[18] K. Yamazaki, An attempt to correct strain data measured with vault-housed extensometers under variations in temperature, Tectonophysics 599 (2013) 89-96.

[19] L. Pei, G. Blöcher, H. Milsch, G. Zimmermann, H. Zhang, X. Li, E. Huenges, Analysis of measured thermally induced rock deformation, Meas.: J. Int. Meas. Confed. 163 (2020) 108004.

[20] L. Pei, G. Blöcher, H. Milsch, G. Zimmermann, I. Sass, E. Huenges, Thermo-mechanical properties of Upper Jurassic (Malm) carbonate rock under drained conditions, Rock Mech. Rock Eng. 51 (2018) 23-45.

[21] R.B. McLellan, T. Ishikawa, The elastic properties of aluminum at high temperatures, J. Phys. Chem. Solids. 48 (1987) 603–606.

[22] S. Homuth, A. E. Götz, I. Sass, Lithofacies and depth dependency of thermo- and petrophysical rock parameters of the Upper Jurassic geothermal carbonate reservoirs of the Molasse Basin, Zeitschrift der Deutschen Gesellschaft für Geowissenschaften 165 (2014) 469-486.

[23] K. Menberg, F. Heberle, C. Bott, D. Brüggemann, P. Bayer, Environmental performance of a geothermal power plant using a hydrothermal resource in the Southern German Molasse Basin, Renew. Energ. 167 (2021) 20-31.

[24] M. Lion, F. Skoczylas, B. Ledesert, Effects of heating on the hydraulic and poroelastic properties of bourgogne limestone, Int. J. Rock Mech. Min. Sci. 42 (2005) 508–520.

[25] H. Yavuz, S. Demirdag, S. Caran, Thermal effect on the physical properties of carbonate rocks, Int. J. Rock Mech. Min. Sci. 47 (2010) 94–103.

[26] H.S. Carslaw, J.C. Jaeger, Conduction of Heat in Solids, Oxford University Press, Oxford, 1986.

[27] F.P. Incropera, D.P. Dewitt, T.L. Bergman, A.S. Lavine, Fundamentals of Heat and Mass Transfer, John Wiley & Sons, Hoboken, 2007.

[28] P. Kosky, R.T. Balmer, W.D. Keat, G. Wise, Exploring Engineering: An Introduction to Engineering and Design, Academic Press, Amsterdam, 2012.

[29] K.V.K. Rao, S.V.N. Naidu, K.S. Murthy, Precision lattice parameters and thermal expansion of calcite, J. Phys. Chem. Solids 29 (1968) 245-248.

[30] J.H. Dellinger, The temperature coefficient of resistance of copper, J. Franklin Inst. 170 (1910) 213-216.

[31] J.C. Jaeger, N.G.W. Cook, R.W. Zimmerman, Fundamentals of Rock Mechanics, Blackwell, Oxford, 2007.

[32] V. Gräf, M. Jamek, A. Rohatsch, E. Tschegg, Effects of thermal-heating cycle treatment on thermal expansion behaviour of different building stones, Int. J. Rock Mech. Min. 64 (2013) 228–235.

[33] J. Walsh, Theoretical bounds for thermal expansion, specific heat and strain energy due to internal stress, J. Geophys. Res. 78 (1973) 7637-7646.

[34] R.A. Fine, F.J. Millero, Compressibility of water as a function of temperature and pressure, J. Chem. Phys. 59 (1973) 5529-5536.

[35] D.P. Dandekar, A.L. Ruoff, Temperature dependence of the elastic constants of calcite between 160 K and 300 K, J. Appl. Phys. 39 (1968) 6004-6009.

[36] R. Hill, Elastic properties of reinforced solids: some theoretical principles, J. Mech. Phys. Solids 11 (1963) 357-372.

[37] F. Thomas, Jr. Irvine, M.R. Duignan, Isobaric thermal expansion coefficients for water over large temperature and pressure ranges, Int. Commun. Heat Mass 12 (1985) 465-478.

[38] R.S. Krishnan, R. Srinivasan, S. Devanarayanan, Thermal Expansion of Crystals, Pergamon Press, Oxford, 1979.

[39] K. Hoffmann, An Introduction to Measurements using Strain Gages, Hottinger Baldwin Messtechnik GmbH, Darmstadt, 1989.

Appendices

A. Working mechanism of the clip-on extensometers

The working mechanism of the extensometers is illustrated in Fig. A.1. As a sample deforms, the two metal cones of an extensometer clipping on the sample are displaced relative to each other. A metal chip in the extensometer is consequently arched shortening the two resistive strain gauges fixed on the concave side of the chip and elongating the two counterparts on the convex side. The thereby changed resistances of these strain gauges give rise to an output potential V_d from the circuit bridging the four gauges. This output potential is sequentially enhanced by a primary amplifier and a secondary one for counting the relative displacement of the two metal cones D_{mea} which represents the change in the sample dimension. The enhanced output potential V_{op} and the primary amplification factor A_p of the functioning circuitry of an extensometer read $V_{op} = V_d\, A_p\, A_s$ and $A_p = R_v/(R_{in} + R_{out})$, respectively.

Therein, A_s, R_v, in this order, represent the gain of the secondary amplifier and the resistance of a rheostat (Table A.1). R_{in}, R_{out} denote the fractal resistances of the in-cell piece and the out-cell piece in the copper wire leading the bridging of the strain gauges to the primary amplifier, respectively (Table A.1; Fig. A.1d). Each strain gauge as adhered to the metal chip was coated using epoxylite. The coating material was in contact with the silicone oil in the triaxial cell during the present temperature cycling tests. Thus, the interferences of air humidity and vacuum on the strain gauges as claimed in [39] was considered not to be relevant to the present study. More technical details of the extensometers can be referenced in [19].

B. Simulated heterogeneous temperature in the triaxial cell

The four types of flux boundaries as applied in the 2-D modelling are depicted as follows. A no-flux boundary (B3) was defined at the upper outer surface of the triaxial cell taking into account the insulation effect of the coating material (Fig. B.1a). A flux boundary as segmented with respect to time (B4) was applied to the lower outer surface of the cell. This boundary (B4) delivered zero flux in the heating process addressing the insulation effect as imposed by the coating material. The boundary (B4) also yielded an efflux out of the cell in the cooling process dealing with the therein applied ventilation and the so induced forced air convection as the coating was partly open. Another time-segmented flux boundary (B5) was defined at the bottom and the base plate of the triaxial cell and at the lower surface of the loading frame. Thereby, the effects of the free air convection in the heating process and the forced air convection in the cooling process could be addressed in modelling, respectively. The last flux boundary (B6) was applied to the remaining outer surface of the loading frame considering the free air convection at this boundary throughout the conducted tests. The aforementioned heat flux by air convection was simulated using the differential temperature of the apparent value in the setup to the average ambient temperature

and the convective heat transfer coefficient (Table B.1). Not least, the bottom plate of the triaxial cell and the underlying base plate contained some hollow space for arranging the cables of the extensometers etc. Hence, a thermal contact (C1) was defined at the interface between the two plates (Figs. 1, B.1a). Such thermal contact dealt with the weakened heat transition between the two plates due to the thin layer of air as embedded at the contact. The thickness of the thin layer of air was assigned 100 µm, which was approximated by averaging the volume of the hollow space in the both plates over the apparent area of the contact (πr_p^2) between the two plates. Therein, r_p denotes the radius of the bottom plate beneath the cell.

The simulated temperature distribution in the triaxial cell differed from the case in the base plate beneath the cell in terms of the magnitudes. At the onset of the cooling ramp in the test on the aluminum alloy, the temperature within the cell ranged from 70 °C on the middle top to 98 °C at the thermal resistors. In contrast, the concurrent temperature in the base plate ranged from 70 °C at the outer boundaries to 74 °C in the lower middle (Fig. B.2a). By the end of this test, the temperature within the cell appeared to be recovered to approximately 30 °C while the temperature in the base plate remained above 41 °C up to 55 °C (Fig. B.2b). Similarly, the temperature in the triaxial cell ranged from 36 °C to 42 °C while the temperature in the base plate ranged from 42 °C to 45 °C at the onset of the cooling ramp in the test on the limestone (Fig. B.2c). By the end of this test, the temperature in the cell returned to approximately 30 °C and the temperature in the middle base plate remained at 34 °C (Fig. B.2d).

We evaluated the effect of thermal radiation on the temperature field in the triaxial cell via including in the modelling the radiation between the inner surface of the cell and the surface of the sample-extensometer setup. The so derived temperature distribution within the cell showed deficits of below 0.1 °C to the results of the present simulation excluding this radiation effect. Thus, the heat transition within the triaxial cell via thermal radiation was considered to be negligible in the present study.

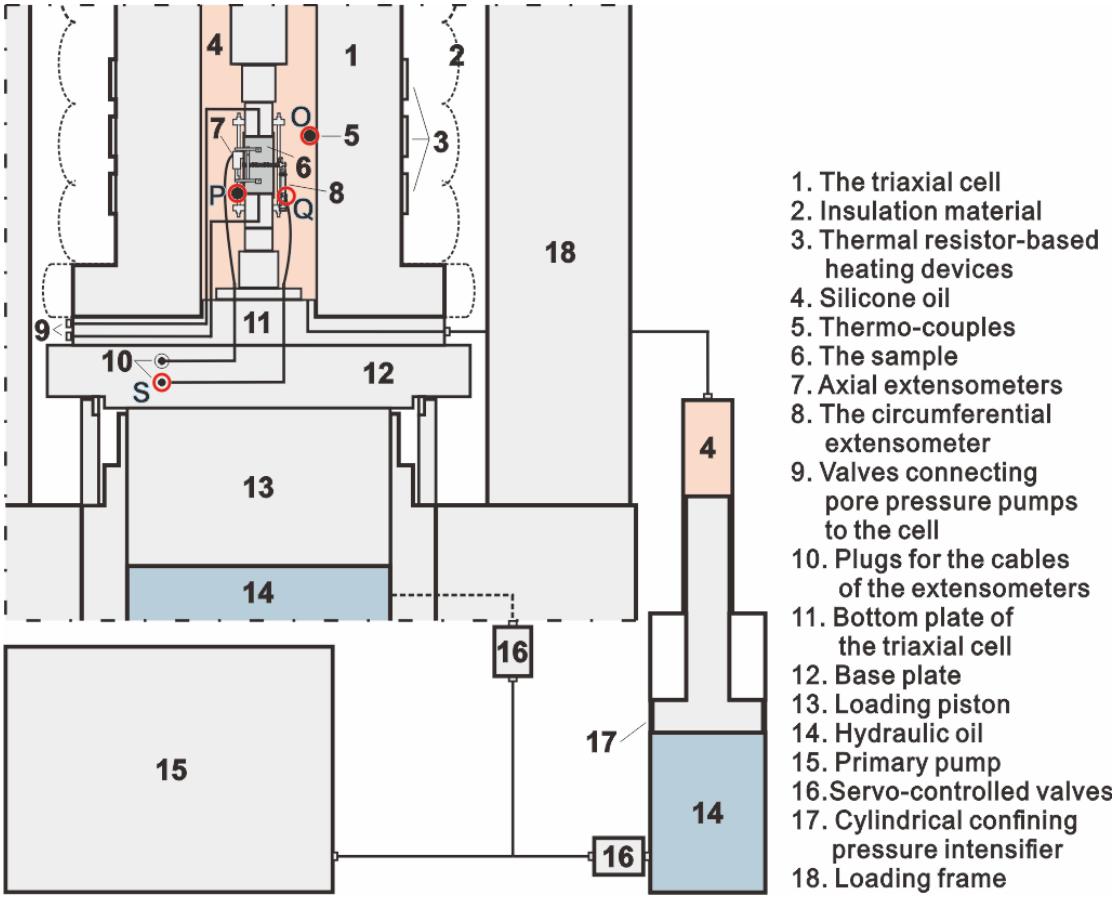

Fig. 1. Schematic diagram showing the setup of the mechanical testing system (MTS) and the specified positions (red circled). In the positions, the plug-in temperature (S), the cell temperature at an extensometer (Q) and at the thermal couples (O, P) were evaluated, respectively.

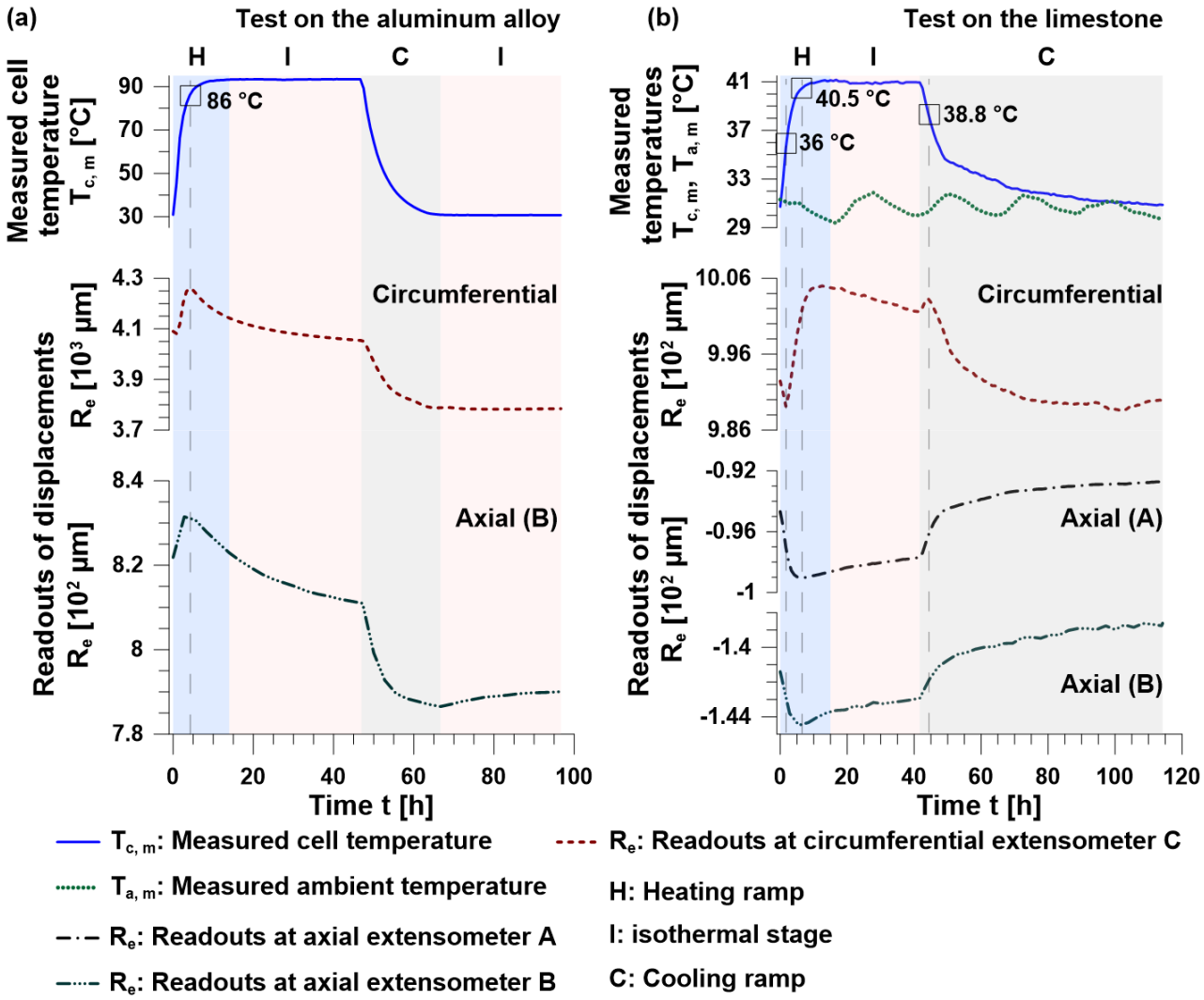

Fig. 2. The monitored displacements reflecting the variations in the sample dimensions throughout the temperature cycling tests on the samples of aluminum alloy (a) and limestone (b). The temperatures logged in both tests are presented in addition.

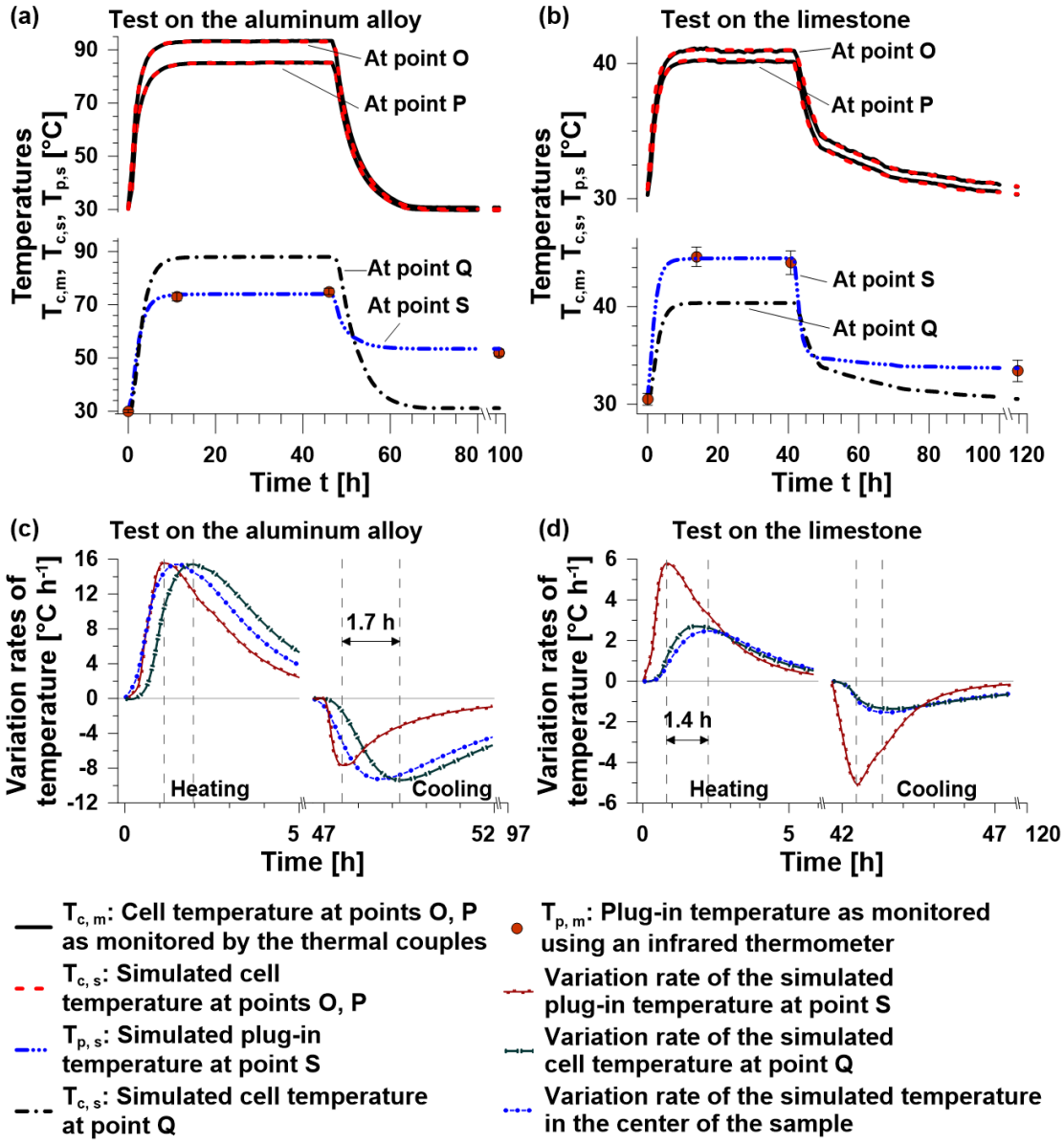

Fig. 3. Measured and simulated temperatures in the mechanical testing system showing heterogeneity (a, b). The simulated cell temperature at the points O, P and the plug-in temperature at the point S in the system were well comparable to the measurements with the thermal couples and the infrared thermometer, respectively. The simulated plug-in temperature appeared to be irreversible in contrast to the simulated cell temperature at the point Q. The positions of these specified points were illustrated in Fig. 1. The vertical error line represented the deviation of the measured plug-in temperature from the average of the measurements. The plug-in temperature varied prior to the temperatures at the point Q and in the center of the samples (c, d).

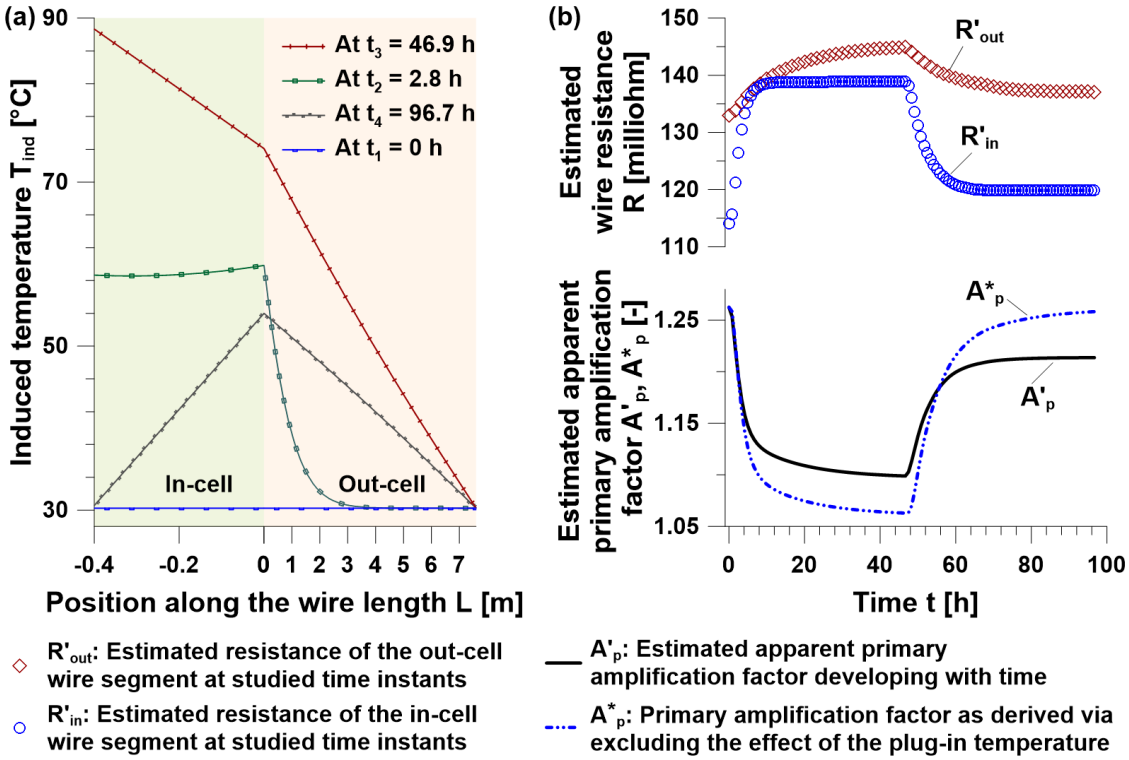

Fig. 4. Simulated temperature distribution in the wire connecting the strain gauges in the axial extensometer B to the amplifiers during the temperature cycle on the aluminum alloy (a). The apparent primary amplification factor A'_p resulted from the varying resistances of the in-cell and the out-cell wire pieces throughout the same temperature cycle (b). The primary amplification factor A^*_p as estimated via excluding the effect of the plug-in temperature is illustrated for reference.

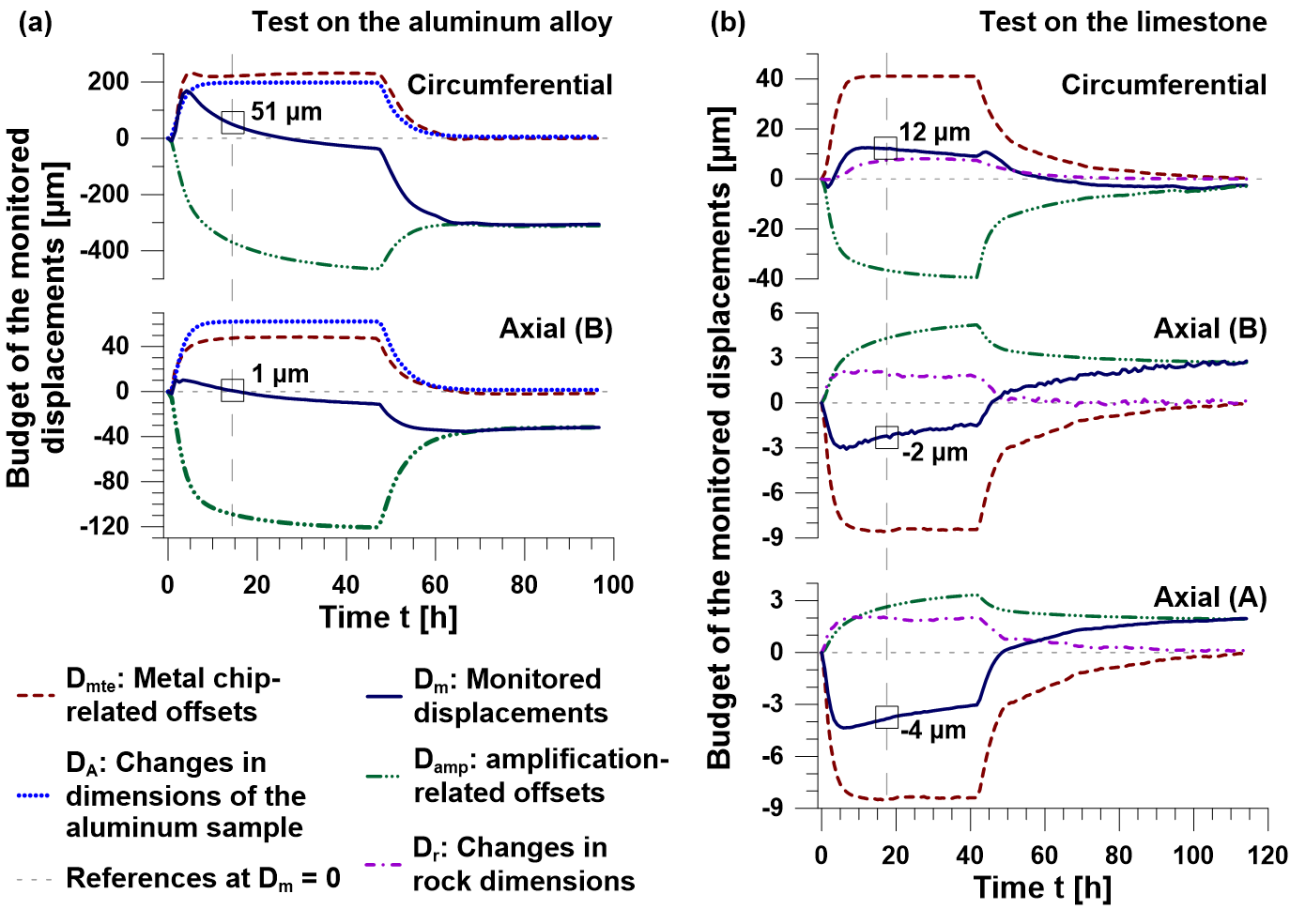

Fig. 5. The amplification- and the metal chip-related offsets as well as the changes in the sample dimensions constituting the displacements as monitored in the temperature cycles on the aluminum alloy (a) and the limestone (b).

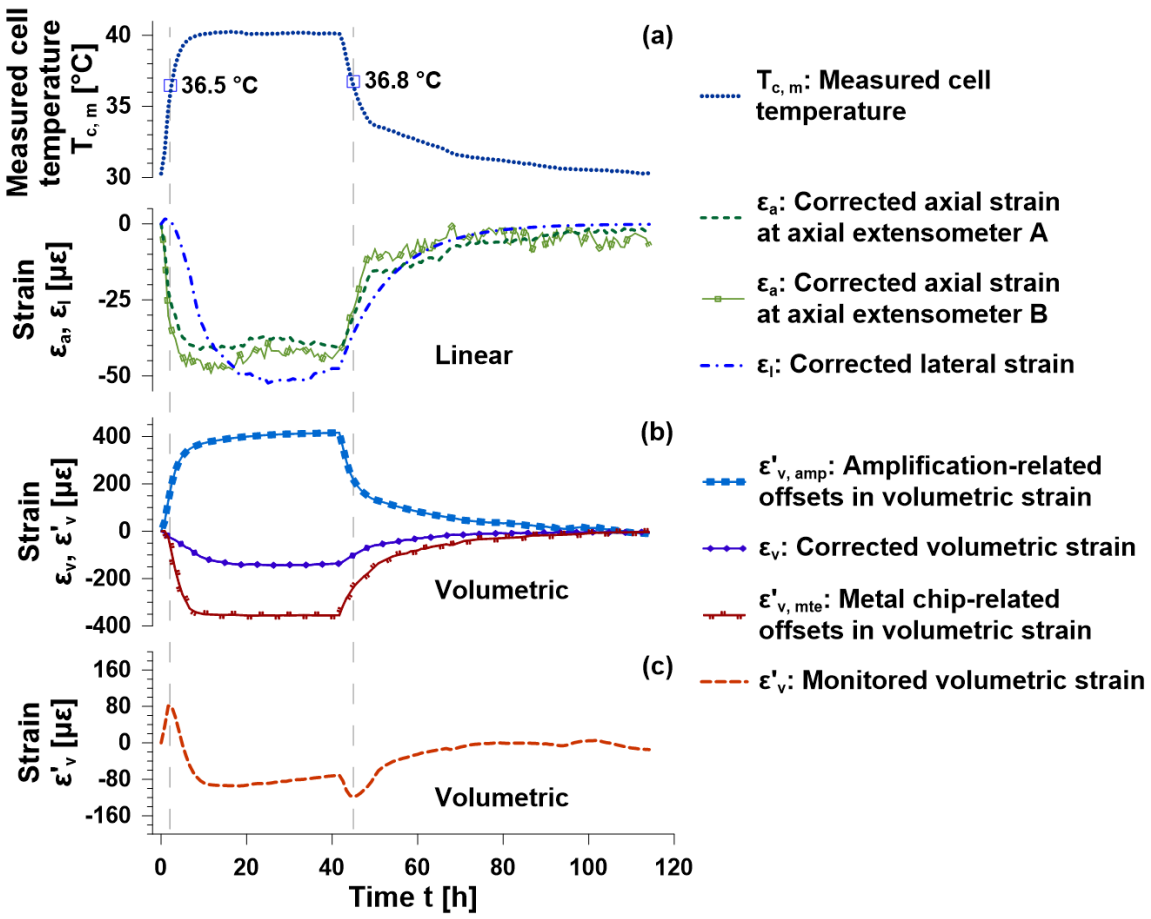

Fig. 6. Rectified linear thermal strain in the present sample of limestone (a). The interplay amongst the rectified volumetric sample strain as well as the strain offsets pertaining to the amplification and the metal chips resulted in the monitored sampe strain (b, c).

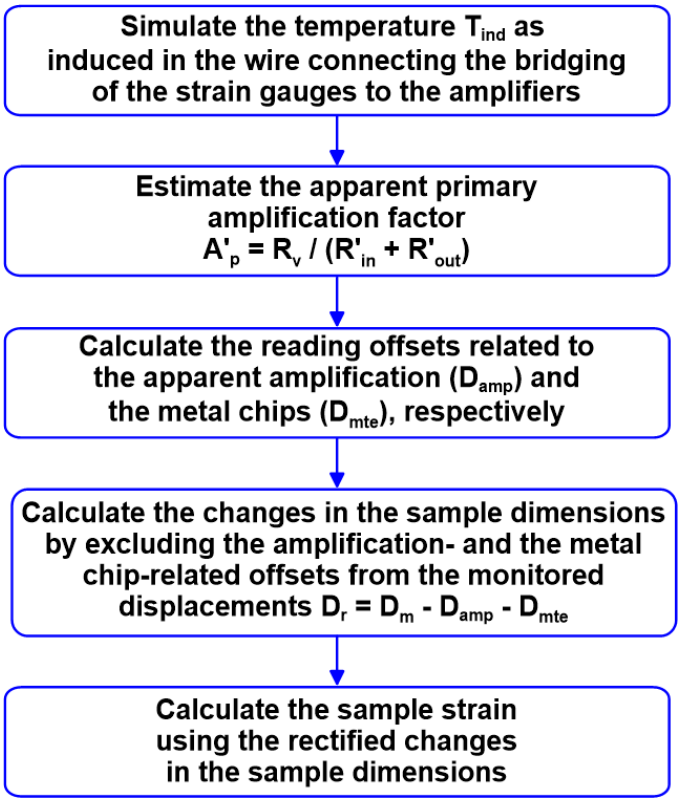

Fig. 7. Diagram summarizing the steps for rectifying the variations in the sample dimensions and for deriving the sample strain.

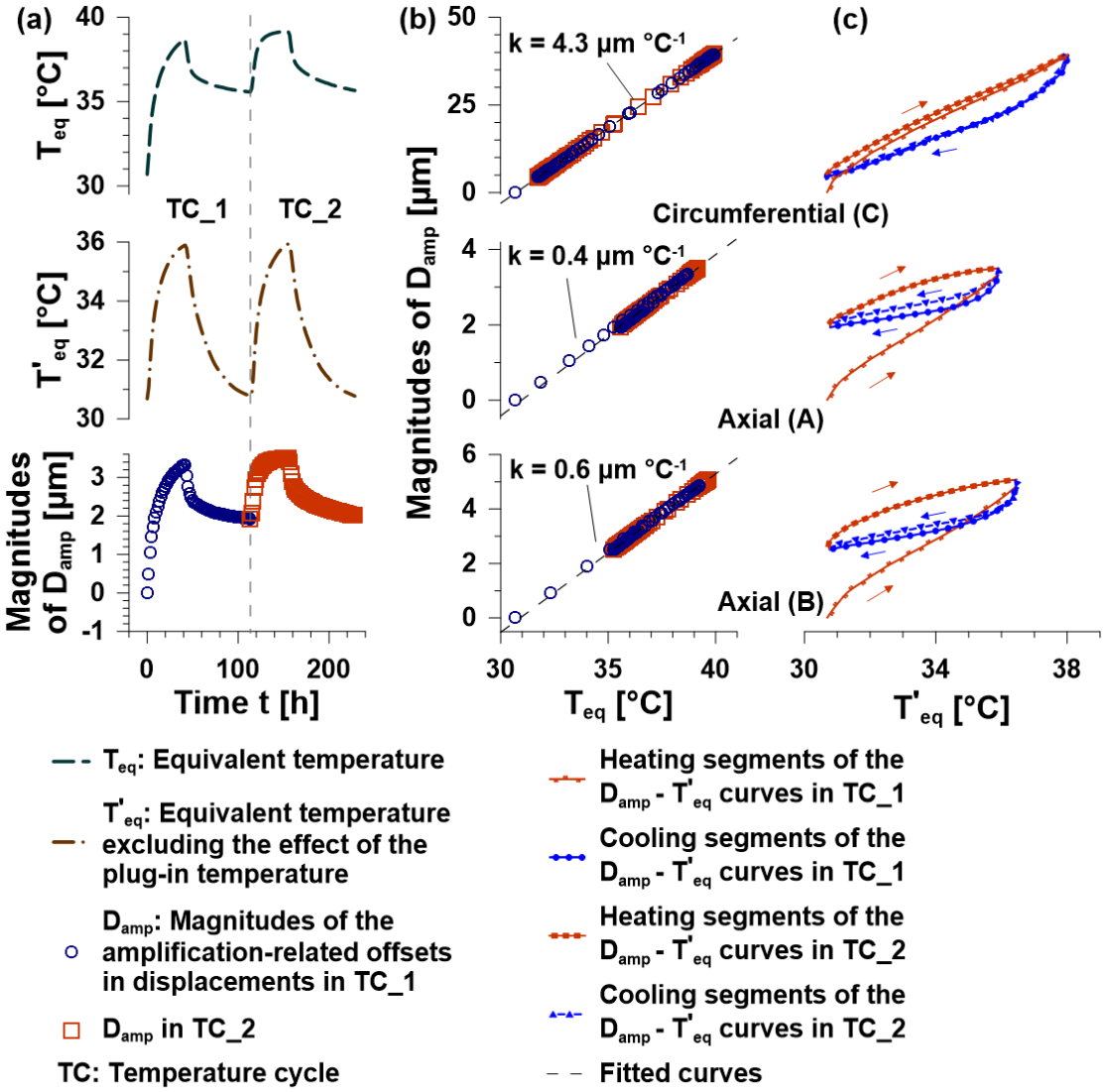

Fig. 8. The magnitudes of the amplification-related offsets D_{amp} in the temperature cycle on the limestone showing consistent tendency of development to the equivalent wire temperature T_{eq} (TC_1; a). Therein, the equivalent temperature T'_{eq} as obtained by excluding the effect of the plug-in temperature was illustrated for comparison. The magnitudes of the offsets D_{amp} manifested linear dependences on the equivalent temperature T_{eq} (b). The heating and cooling segments of the D_{amp}-T'_{eq} curves showed hysteresis (c) as the effect of the plug-in temperature was neglected when the temperature T'_{eq} was derived. In the modelled second temperature cycle on the same sample (TC_2), the dependences of the offsets D_{amp} on the temperature T_{eq} showed consistency to the case in the first experimentally conducted cycle (TC_1). Throughout the two temperature cycles, the hysteresis amongst the segments in the D_{amp}-T'_{eq} curves could develop (c).

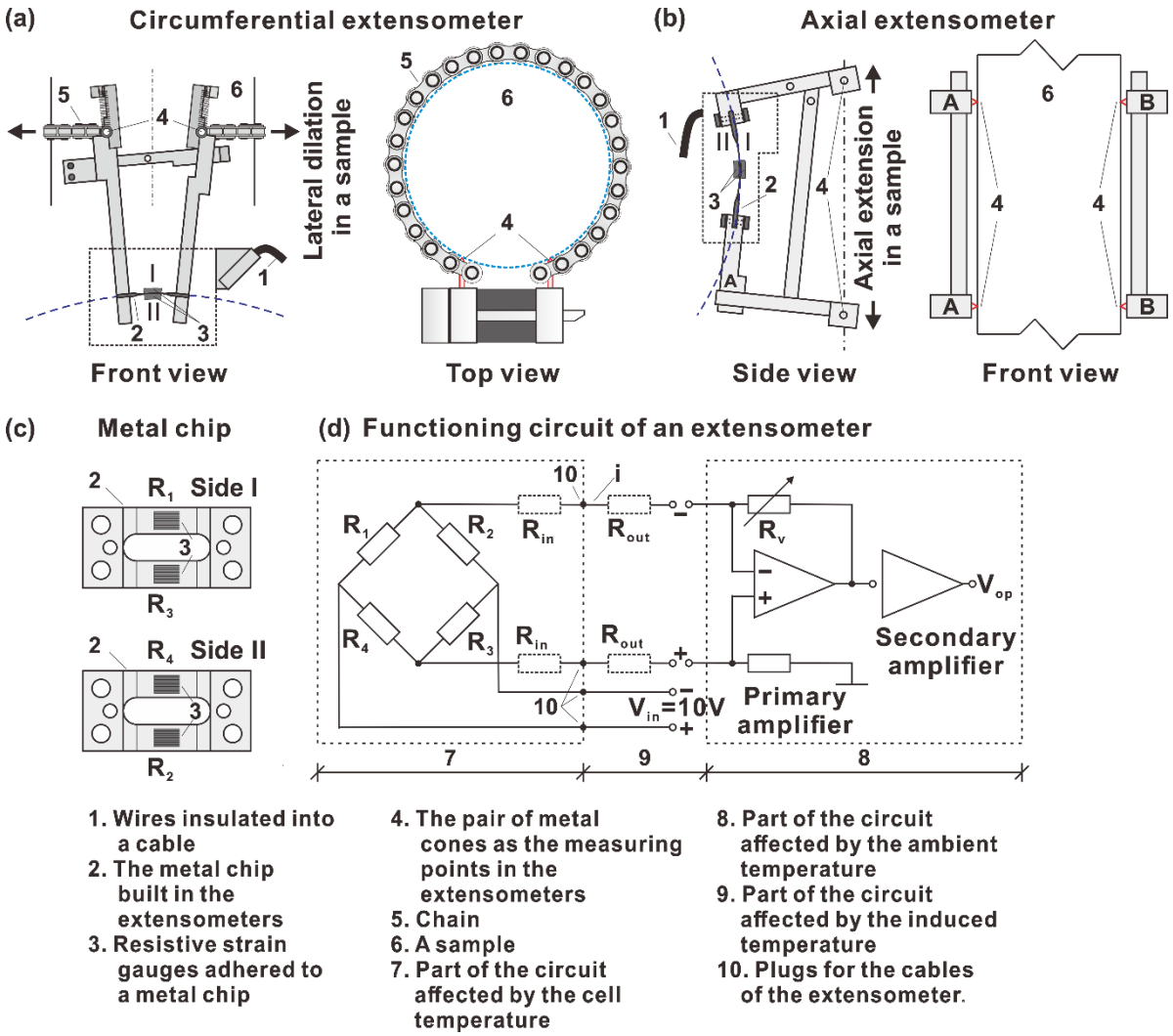

Fig. A.1. Working mechanism of the clip-on extensometers. The changes in the sample dimension displaced the pair of metal cones of an extensometer bulging a metal chip (a, b). The thereby deformed resistive strain gauges fixed on the chip (c) led to an output voltage from the circuit bridging the strain gauges. This output voltage was amplified by the primary and the secondary amplifiers, and equilibrated into the measured displacements (d). Updated based on [19].

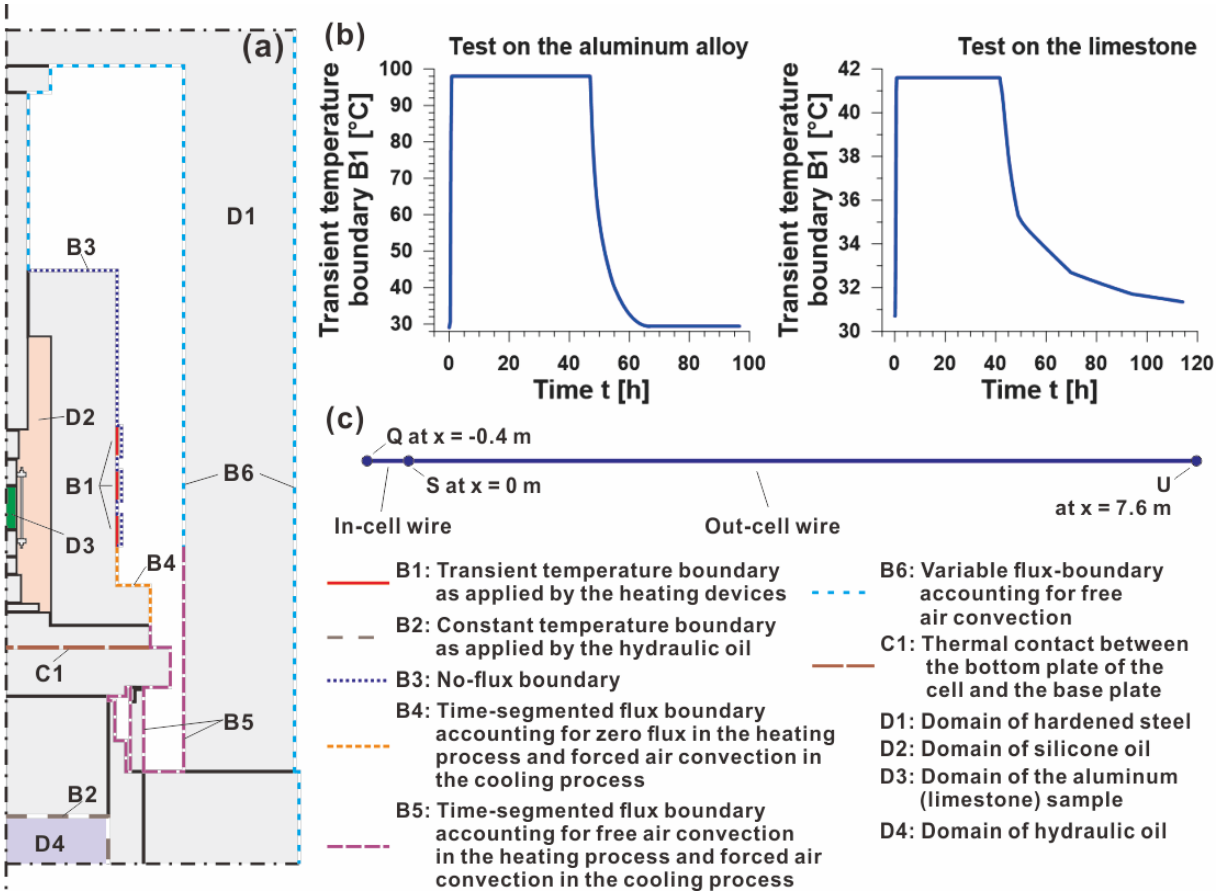

Fig. B.1. Schematic diagram illustrating the setup of a 2-D numerical model of the mechanical testing system (a), the temperature cycles as predetermined at the heating devices (b) and the setup of a 1-D line model (c). The 2-D model (a) was defined into four domains (D1-D4) showing the applied boundaries of temperature (B1, B2) and heat flux (B3-B6) as well as a thermal contact (C1). The 1-D line model (c) represented a wire that led the bridging of the strain gauges to the amplifiers. This wire was fed into the triaxial cell through the plug S leaving the end U at ambient temperature, and was connected to the strain gauges at the end Q.

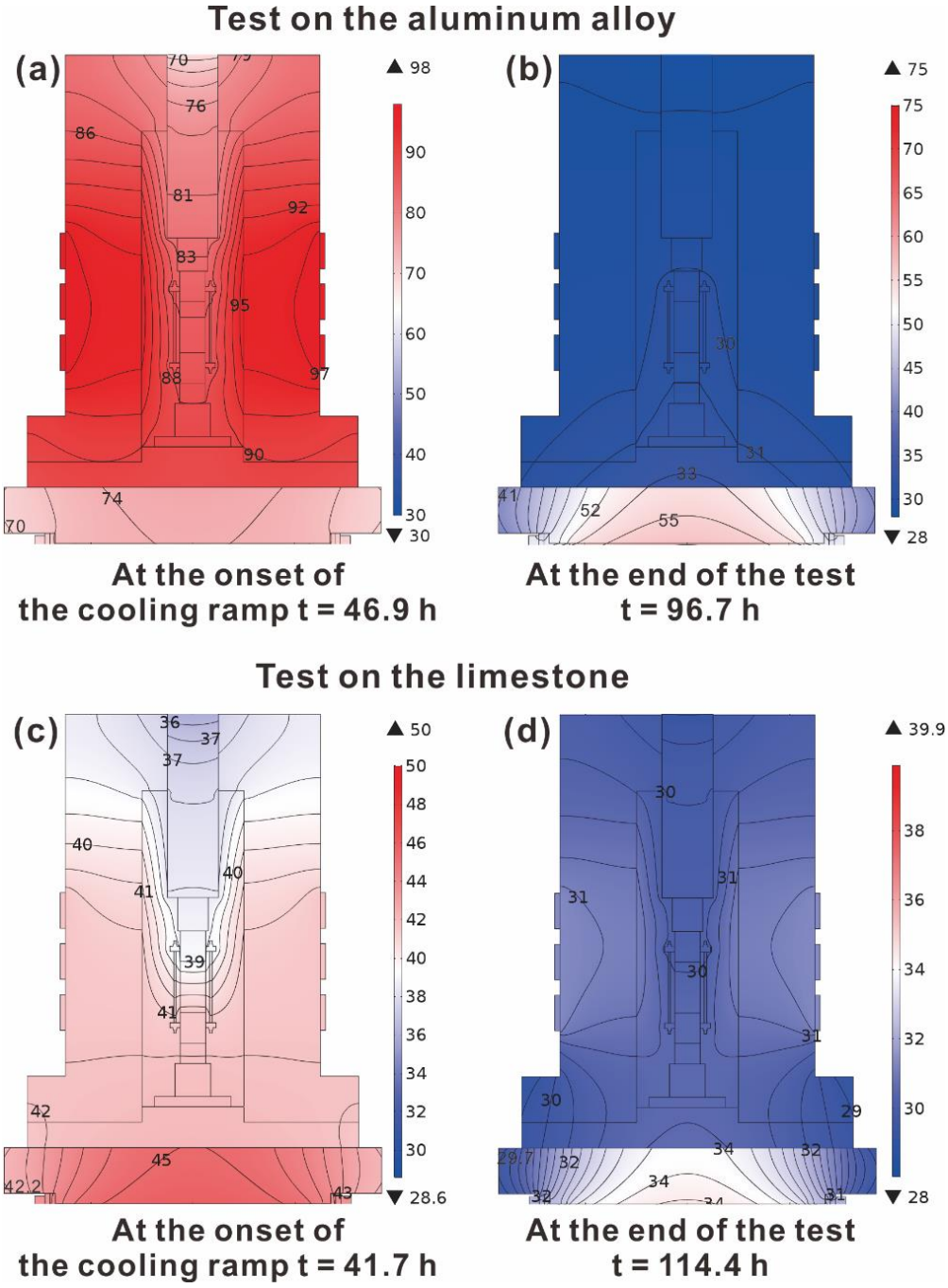

Fig. B.2. Simulated heterogeneous temperature as distributed in the setup of the triaxial cell at specified time instants during the temperature cycles on the aluminum alloy (a, b) and the limestone (c, d), respectively.

Table 1

Values of the material properties at specified temperatures as applied in the numerical modelling (*).

Materials	Thermal conductivity [W m^{-1} °C^{-1}]			Specific heat capacity [J kg^{-1} °C^{-1}]			Density [kg m^{-3}]		
	30	40	90	30	40	90	30	40	90
Hardened steel	64	64	65	461	465	484	7860	7860	7857
Silicone oil	0.25	0.25	0.23	2170	2230	2396	861	849	817
Hydraulic oil	0.12	0.12	0.12	2040	2096	2252	847	847	845
Aluminum alloy	122	124	134	850	858	893	2754	2754	2751
Limestone	2.17	2.11	1.93	775	788	847	2680	2642	2623
Air	0.026	0.027	0.031	1004	1007	1010	1.15	1.13	0.97

(*) The values of the material properties were referred to the dataset as archived in COMSOL.

Table 2

Segments of the displacements as monitored in the present temperature cycles (*).

Temperature cycle on the aluminum alloy					Temperature cycle on the limestone					
Thermal path	Displacements		Extensometers		Thermal path	Displacements		Extensometers		
			Cir. C	Axial B				Cir. C	Axial A	Axial B
30 °C to 90 °C	D_m	[μm]	51	1	30 °C to 40 °C	D_m	[μm]	12	-4	-2
	D_{amp}		-378	-109		D_{amp}		-36	3	4
	D_{mte}		231	48		D_{mte}		41	-9	-8
	D_A		198	62		D_r		7	2	2
At 90 °C	D_m	[μm]	-87	-12	At 40 °C	D_m	[μm]	-3	1	1
	D_{amp}		-87	-12		D_{amp}		-3	1	1
	D_{mte}		0	0		D_{mte}		0	0	0
	D_A		0	0		D_r		0	0	0
90 °C to 30 °C	D_m	[μm]	-267	-24	40 °C to 30 °C	D_m	[μm]	-12	5	4
	D_{amp}		162	86		D_{amp}		36	-2	-2
	D_{mte}		-231	-48		D_{mte}		-41	9	8
	D_A		-198	-62		D_r		-7	-2	-2
At 30 °C	D_m	[μm]	-3	3	At 30 °C	D_m	[μm]	-	-	-
	D_{amp}		-3	3		D_{amp}		-	-	-
	D_{mte}		0	0		D_{mte}		-	-	-
	D_A		0	0		D_r		-	-	-

(*) D_m , D_{amp} , D_{mte} denote sequentially the monitored displacements, the amplification- and the metal chip-related offsets. D_A, D_r represent the displacements due to the dimensional changes of the samples of aluminum alloy and limestone, respectively.

Table A.1

Parameters relevant to the functioning of the clip-on extensometers (*).

Extensometers	Amplification factor of the primary amplifier A_p [-]	Resistance of rheostat R_v [milliohm]	Measured resistance of the in-cell wire piece R_{in} [milliohm]	Measured resistance of the out-cell wire piece R_{out} [milliohm]	Increase in wire resistance per unit change in temperature (**) γ [10^{-3} °C^{-1}]
Axial A	1.31	250	60	130	4.26
Axial B	1.26	310	110	130	4.26
Circumferential C	1.04	170	30	130	4.26

(*) The values were determined at 30 °C.

(**) The values evaluating the temperature dependence of the resistance of copper wire were quoted from [30].

Table B.1

Values of the convective heat transfer coefficient as applied to the flux boundaries in the 2-D numerical model (*).

Flux boundaries	Convective heat transfer coefficient [W m^{-2} °C^{-1}]	
	Heating process	Cooling process
B3	0	0
B4	0	250
B5	10	250
B6	10	10

(*) The values of the convective heat transfer coefficient were referred to [27, 28].